Effects of strong magnetic fields on pairing fluctuations in high-temperature superconductors

M. Eschrig

Department of Physics & Astronomy, Northwestern University, Evanston, Illinois 60208

D. Rainer

Physikalisches Institut, Universität Bayreuth, D-95440 Bayreuth, Germany

J. A. Sauls

Department of Physics & Astronomy, Northwestern University, Evanston, Illinois 60208

We present the theory for the effects of superconducting pairing fluctuations on the nuclear spin-lattice relaxation rate $1/T_1$ and the NMR Knight shift for layered superconductors in high magnetic fields. These results can be used to clarify the origin of the pseudogap in high-T_c cuprates, which has been attributed to spin fluctuations as well as pairing fluctuations. We present theoretical results for s-wave and d-wave pairing fluctuations and show that recent experiments in optimally doped YBa$_2$Cu$_3$O$_{7-\delta}$ are described by d-wave pairing fluctuations [V. F. Mitrović *et al.*, Phys. Rev. Lett. **82**, 2784 (1999); H. N. Bachman *et al.* (unpublished)]. In addition, we show that the orthorhombic distortion in YBa$_2$Cu$_3$O$_{7-\delta}$ accounts for an experimentally observed discrepancy between $1/T_1$ obtained by nuclear quadrupole resonance and nuclear magnetic resonance at low field. We propose an NMR experiment to distinguish a fluctuating s-wave order parameter from a fluctuating strongly anisotropic order parameter, which may be applied to the system Nd$_{2-x}$Ce$_x$CuO$_{4-\delta}$ and possibly other layered superconductors. [S0163-1829(99)02818-0]

I. INTRODUCTION

Fluctuations are enhanced in high-T_c cuprate superconductors because of their layered structure and their small coherence length.[3] In contrast to conventional superconductors, where the transition is very well described by a mean-field theory, an extended region of one to several Kelvin around the transition is expected to be dominated by critical fluctuations in the cuprates. In this paper we discuss the effects of Gaussian dynamical fluctuations above T_c, which are observable over a temperature range $T-T_c \approx T_c$, on the nuclear spin-lattice relaxation rate and the NMR Knight shift in high-T_c superconductors. For a comprehensive review on the role of NMR and nuclear quadrupole resonance (NQR) spectroscopy in the study of fluctuation effects in high-T_c superconductors, see Rigamonti, Borsa, and Carretta.[4]

Pairing fluctuation effects on the spin-lattice relaxation rate have been investigated in the dirty limit for static, long-wavelength fluctuations near T_c by Kuboki and Fukuyama.[5] Heym extended these calculations for s-wave pairing fluctuations by including the fluctuation corrections to the quasiparticle density of states.[6] Analytic expressions for the static, long-wavelength fluctuation corrections to the spin-lattice relaxation rate and Knight shift were obtained by Randeria and Varlamov for ultraclean and dirty s-wave superconductors.[7] We extend their calculations to include finite magnetic fields and unconventional pairing for general values of the impurity scattering rate. Our calculations and numerical results include dynamical fluctuations and short-wavelength fluctuations summed over all Landau levels.

Dynamical quantities such as the fluctuation contribution to the spin-lattice relaxation rate $1/T_1$ carry valuable information on the type of fluctuations and characteristic scatter-

ing rates and lifetimes. Qualitatively different behavior for the fluctuation contributions to the rate is predicted for different symmetries of the order-parameter fluctuations.[8] Analysis of the fluctuation corrections to $1/T_1$ provides information on the elastic- and inelastic-scattering parameters. The *sign* of the fluctuation corrections to $1/T_1$ is sensitive to pair breaking and the symmetry of the pairing fluctuations; thus nonmagnetic impurities have almost no pair breaking effect on fluctuations with s-wave symmetry, but have strong effects for d-wave pairing. In the case of s-wave pairing a large positive fluctuation contribution to $1/T_1$ originates from the anomalous Maki-Thompson (MT) process.[9,5] We show that this process is suppressed in zero field almost completely for d-wave pairing if the mean free path is shorter than 20 coherence lengths, but cannot be neglected near the transition in finite magnetic fields or in the ultraclean limit. Fluctuation corrections to the quasiparticle density of states (DOS) dominate the anomalous Maki-Thompson processes in the case of d-wave pairing symmetry for realistic scattering parameters in high-T_c cuprates. For a recent review on the role of pairing fluctuation corrections to the quasiparticle density of states in high-T_c superconductors, see Varlamov *et al.*[10]

Recent ^{63}Cu NQR-NMR experiments on optimally doped YBCO by Carretta *et al.*[8] were interpreted in terms of a pseudogap originating from superconducting fluctuations. Other theories for the pseudogap include spin-charge separation, preformed pairs, phase fluctuations, and van Hove scenarios. For a recent review of this broad topic and references, see Randeria.[11] Chubukov, Pines, and Stojkovic[12] proposed a magnetic mechanism for the pseudogap in which "hot" quasiparticles become gapped by a precursor spin-density wave. Recent studies by Auler *et al.*[13] of ^{63}Cu and ^{89}Y NMR in
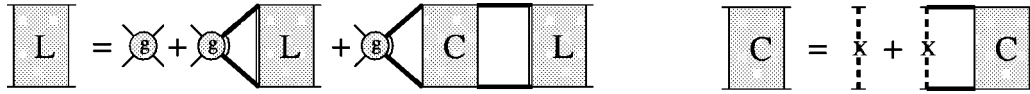
FIG. 1. Left: Diagrammatic representation of the Bethe-Salpeter equation for the fluctuation propagator L. The vertex g represents the pairing interaction, the thick solid lines are quasiparticle Green's functions, and the block vertex C represents vertex corrections due to impurity scattering. Thin double lines symbolize vertex factors $\eta(\psi)$ due to the anisotropy of the pairing interaction. Right: Diagrammatic representation of the Bethe-Salpeter equation for the impurity vertex corrections. A thick crossed line stands for the impurity scattering vertex in the Born approximation. The analytic forms for these equations are given in Eqs. (6) and (3).

YBCO as a function of doping were interpreted as evidence for the vanishing of the pseudogap for hot quasiparticles due to antiferromagnetic spin fluctuations exactly at optimal doping, whereas a pseudogap for ''cold'' quasiparticles persisted at optimal and overdoped samples. Whether the pseudogap is due to pairing fluctuations, spin-density wave fluctuations, or more complicated mechanisms may not be easy to decide, especially in optimally doped materials. The study of fluctuation effects in the presence of strong magnetic fields may be key to solving this problem.

Magnetic fields tend to enhance pairing fluctuations near the transition temperature as a result of Landau quantization of the orbital motion of pairs.[14] However, because the transition temperature is suppressed by a magnetic field, pairing fluctuations are typically reduced at constant temperature with increasing field. Application of a magnetic field at constant temperature has very different effects on the pairing fluctuation contributions to $1/T_1$ depending on the pairing symmetry. For s-wave pairing the rate is reduced with increasing field, whereas in d-wave pairing the suppression of the DOS fluctuations, which have a negative sign, leads to an enhancement of $1/T_1$ with field.[8]

In the next section we describe the theoretical framework for our analysis of fluctuation effects on NMR in high magnetic fields in high-T_c superconductors. We derive the fluctuation propagator for a quasi-two-dimensional (2D) layered superconductor and include quasiparticle scattering by nonmagnetic impurities in addition to pair breaking by inelastic scattering. We incorporate orbital quantization by the magnetic field on the pairing fluctuations as well as the effects of d-wave symmetry. In Sec. III we discuss the pairing fluctuation corrections to the nuclear spin-lattice relaxation (NSLR) rate. To leading order in T_c/E_f the dominant fluctuation corrections are determined by Maki-Thompson processes and corrections to the quasiparticle density of states. We derive expressions for these processes appropriate to 2D fluctuations in a strong magnetic field and present our results for the pairing fluctuation corrections to the NSLR rate. The field dependence of the fluctuations is shown to be sensitive to the symmetry of the pairing fluctuations. In Sec. IV we derive the leading-order corrections to the Pauli spin susceptibility and its contribution to the Knight shift. The Knight shift is determined by the the long-wavelength spin susceptibility, and in contrast to the NSLR rate the fluctuation corrections to the spin susceptibility are not very sensitive to order-parameter symmetry or impurity scattering. However, dynamical fluctuations and orbital quantization lead to significant effects on both the rate and the spin susceptibility which are essential for a quantitative understanding of the pseudogap behavior in high-T_c cuprates. In Secs. III and IV we compare our theoretical results with recent measurements of the pseudogap in the NSLR rate and the Knight shift

performed by Mitrović $et\ al.$[1] and Bachman $et\ al.$[2] on optimally doped YBCO in magnetic fields up to 30 T. We show that the pseudogap in optimally doped YBCO can be accounted for quantitatively by the theory of 2D pairing fluctuations with d-wave symmetry.[1,2] Finally, we show that incorporating orthorhombic anisotropy and the allowed mixing of s-wave and d-wave pairing fluctuation channels leads to a low-field crossover from predominantly s-wave fluctuations to predominantly d-wave fluctuations which provides a natural explanation for the observed evolution from the NQR rate to the low-field (below 2 T) ^{63}Cu NSLR rate on optimally doped YBCO.

II. PAIR PROPAGATOR FOR UNCONVENTIONAL PAIRING

Fluctuating Cooper pairs are described by a propagator L which derives from the sum over ladder diagrams in the particle-particle interaction channel as shown in Fig. 1.[10] Our derivation includes impurity scattering for a layered 2D superconductor with an isotropic Fermi surface and a weak-coupling anisotropic pairing interaction g. The generalization to anisotropic 2D and 3D Fermi surfaces is straightforward.

The propagator is a function of the total momentum $\mathbf{q}$ of a pair of interacting quasiparticles, their total excitation energy ω and, for anisotropic pairing, their relative incoming and outgoing momenta $\mathbf{k}_{in,out}$. In the following we use cylindrical coordinates (q,ϕ,q_z) and write $\mathbf{q}$ as $\mathbf{q} = \{q\cos\phi, q\sin\phi, q_z\}$. Pairing fluctuations are long lived only for small ω and q, so that the two particles which interact have nearly opposite momenta on the Fermi surface, i.e., $\mathbf{k}_{in} \approx 2\mathbf{k}_{F,in}$ and $\mathbf{k}_{out} \approx 2\mathbf{k}_{F,out}$. We assume a cylindrical Fermi surface of radius k_F, in which case the momenta on the Fermi surface are given by $\mathbf{k}_F = \{k_F\cos\psi, k_F\sin\psi, k_z\}$.

The pairing interaction is a function of the momenta of the initial and final state of quasiparticles on the Fermi surface. We denote the angles between the x axis (chosen as the tetragonal $\hat{a}$ axis) and $\mathbf{k}_F$ and $\mathbf{k}_F'$ by ψ and ψ', respectively. The pairing interaction $V(\psi,\psi')$ can be expanded in eigenfunctions belonging to the irreducible representations of the symmetry group of the crystal. We denote the eigenfunction with the largest attractive (positive) eigenvalue by $\eta(\psi)$ and neglect for now the other subdominant interactions in the expansion of V. Thus we write the pairing interaction in the following form:

$$V(\psi,\psi') = \eta(\psi) \cdot g \cdot \eta(\psi'). \tag{1}$$

Note that we can neglect the small difference between $\mathbf{k}_F$ and $\mathbf{k}_F - \mathbf{q}$ in the pairing interaction, since $q \sim 1/\xi_0 \ll k_F$, where $\xi_0 = \hbar v_F / 2\pi k_B T_c$ is the coherence length.

The fluctuation propagator $L(\omega,\mathbf{q})$ describes dynamically fluctuating Cooper pairs with a wavelength $2\pi/q$ and a frequency ω. Near T_c the typical lifetime of a pairing fluctuation in the clean limit is

$$\tau_{GL} = \frac{\hbar\pi}{8k_BT}\left(a\xi_0^2 q^2 + \frac{T-T_c}{T_c} \right)^{-1}, \qquad (2)$$

where $a = 7\zeta(3)/8 \approx 1.05$. We set $\hbar = k_B = 1$ except when explicitly noted.

In the case of strong pair breaking with dephasing time τ_ϕ the prefactor $\hbar\pi/8k_BT$ is replaced by τ_ϕ. Spatially small fluctuations decay faster than more extended fluctuations. Long-lived fluctuations have typical sizes larger than $\xi_0\sqrt{T_c/(T-T_c)}$. When the temperature approaches T_c the importance of long-wavelength ($\mathbf{q}\rightarrow 0$), quasistatic fluctuations ($\omega\rightarrow 0$) increases until fluctuation modes start to overlap in space and time. When this happens fluctuation modes interact, which defines the critical fluctuation regime. In contrast to conventional superconductors, where this regime is negligibly small, it extends over 1–2 K in layered high-T_c cuprates like YBCO.[3] Our analysis neglects interactions between fluctuation modes and thus excludes the critical regime.

We include the effects of impurities via the standard procedure of averaging over impurity positions in the limit of a long mean free path, $l \gg k_F^{-1}$.[15] Impurities lead to three different effects: they introduce a finite quasiparticle lifetime via the electron self-energy, they generate vertex corrections V in the particle-hole channels, which have to be included to ensure fundamental conservation laws, and they generate a Cooperon-like mode in the particle-particle channel, the impurity vertex C, which couples directly to the full pair fluctuation propagator L. In the case of d-wave pairing impurities lead to pair breaking of the pairing fluctuation modes. We will use a shorthand notation $Q \equiv (\omega_l, q, \phi)$ for the set of arguments related to the pairing channel. The impurity vertex (the cross in Fig. 1) is given in terms of the impurity scattering rate in Born approximation, $\tilde{\alpha} = 1/2\pi\tau N_F$:

$$C(\epsilon_n,Q) = \tilde{\alpha} + \tilde{\alpha}A_0(\epsilon_n,Q)C(\epsilon_n,Q), \qquad (3)$$

where $A_0(\epsilon_n,Q)$ is a momentum-averaged irreducible pair susceptibility, defined by the formula (with $m=0$)

$$A_m(\epsilon_n,Q) \equiv A_m(\epsilon_n,\omega_l,q,\phi) = N_F\int_0^{2\pi} d\psi[\eta(\psi)]^m$$

$$\times \int d\xi_{\mathbf{k}}G(\epsilon_n,\xi_{\mathbf{k}})G(\omega_l - \epsilon_n,\xi_{\mathbf{q-k}}). \qquad (4)$$

Here, $\xi_{\mathbf{k}} = \epsilon(\mathbf{k}) - \mu$ is the quasiparticle dispersion relative to the chemical potential. Because $q \ll k_F$, we approximate $\xi_{\mathbf{q-k}} \approx \xi_{\mathbf{k}} - \mathbf{v}_F\cdot\mathbf{q}$. The Matsubara Green's functions are given by

$$G(\epsilon_n,\xi_{\mathbf{k}}) = \frac{1}{i\epsilon_n - \xi_{\mathbf{k}} + \frac{i}{2}\,\mathrm{sign}(\epsilon_n)\left(\frac{1}{\tau}+\frac{1}{\tau_\phi}\right)}, \qquad (5)$$

where $1/\tau_\phi$ is the inelastic-scattering rate and $1/\tau$ is the elastic-scattering rate. We introduce dimensionless scattering parameters $\alpha = \hbar/2\pi\tau k_B T_c$ and $\alpha_\phi = \hbar/2\pi\tau_\phi k_B T_c$. The inelastic-scattering rate contributes to the quasiparticle scattering, but not to the impurity vertex C for the fluctuation propagator. Consequently, the lifetime of the pair fluctuation propagator is governed by τ_ϕ. Note that both scattering parameters α and α_ϕ are defined in terms of the *renormalized* transition temperature $T_c \equiv T_c(\alpha,\alpha_\phi)$, which is given by an Abrikosov-Gorkov formula[15,16] (see Appendix B), so that their values range from zero (for the clean limit) to infinity (e.g., for the critical pair breaking rate). In high-T_c cuprates the mean free path l is typically of the order of 3–10 coherence lengths;[17] a reasonable estimate is $l \approx 5\xi_0$, which corresponds to $\alpha \approx 0.2$. For the pair breaking parameter (or dephasing rate) α_ϕ one usually assumes a much smaller value. For example, comparison between theory and experiment for the $\hat{c}$-axis fluctuation magnetoresistance yields $\tau_\phi T_c \approx 10$ in YBCO and BSCCO, corresponding to $\alpha_\phi \approx 0.02$.[18] An estimate of α_ϕ from inelastic scattering of quasiparticles by phonons yields $\alpha_\phi \approx (k_BT/\hbar\omega_D)^2$, which at T_c in optimally doped cuprates is $\approx 10^{-2}$. However, this weak-coupling estimate of inelastic pair breaking may be inappropriate if the inelastic lifetime is due to strong coupling to low-frequency boson modes. Strong coupling or large inelastic pair breaking can have a strong effect on the pairing fluctuation corrections to the nuclear spin-lattice relaxation rate.[19] In weak-coupling s-wave theory a sign change in the fluctuation corrections to the rate occurs for $\alpha_\phi \approx 0.26$.[20] A similar sign change occurs in strong-coupling theory for a coupling constant $\lambda \approx 2$. Note, however, that a coupling strength of $\lambda \approx 2$ is much larger than that in conventional strong-coupling superconductors like lead. We consider parameters $\alpha_\phi \gtrsim 0.26$ and $\lambda \gtrsim 2$ as unreasonably large for high-T_c cuprates. In high-T_c materials pair breaking by inelastic scattering is probably not strong enough to produce such qualitative changes in the behavior of the fluctuation corrections to the spin-lattice relaxation rate. Thus the remaining discussion focuses on fluctuations in weak-coupling layered superconductors.

For a single pairing channel in an isotropic quasi-2D metal the fluctuation propagator factorizes into $\eta(\psi)L(Q)\eta(\psi')$, where $L(Q)$ obeys the Bethe-Salpeter equation:

$$L(Q) = g + T\sum_n gA_2(\epsilon_n,Q)L(Q)$$

$$+ T\sum_n gA_1(\epsilon_n,Q)C(\epsilon_n,Q)A_1(\epsilon_n,Q)L(Q). \qquad (6)$$

Inserting the Cooperon propagator $C(\epsilon_n,Q)$ from Eq. (3) into Eq. (6) we can solve for $L(Q)$ in terms of the momentum integrated pair susceptibilities $A_m(\epsilon_n,Q)$ to obtain

$$L(Q) = \frac{1}{g^{-1} - T\Sigma_n B_2(\epsilon_n, Q)}, \qquad (7)$$

where

$$B_2(\epsilon_n, Q) = A_2(\epsilon_n, Q) + A_1(\epsilon_n, Q)^2 C(\epsilon_n, Q)$$

$$= \frac{A_2(\epsilon_n, Q) + \tilde{\alpha}[A_1^2 - A_0 A_2](\epsilon_n, Q)}{1 - \tilde{\alpha} A_0(\epsilon_n, Q)}. \qquad (8)$$

Finally, we must include impurity vertex corrections in the particle-particle channel to the external vertices of the pair propagator. These corrections are incorporated by the replacement $\eta L \eta' \to K$ with

$$K(\epsilon_n, \epsilon_{n'}, \psi, \psi', Q) = \tilde{\eta}(\epsilon_n, \psi, Q) \cdot L(Q) \cdot \tilde{\eta}(\epsilon_{n'}, \psi', Q), \qquad (9)$$

where

$$\tilde{\eta}(\epsilon_n, \psi, Q) = \eta(\psi) + A_1(\epsilon_n, Q) C(\epsilon_n, Q). \qquad (10)$$

Combined with Eq. (3) this gives

$$\tilde{\eta}(\epsilon_n, \psi, Q) = \frac{\eta(\psi) + \tilde{\alpha}(A_1(\epsilon_n, Q) - \eta(\psi) A_0(\epsilon_n, Q))}{1 - \tilde{\alpha} A_0(\epsilon_n, Q)}. \qquad (11)$$

In the case $\eta(\psi) \equiv 1$ we recover the standard vertex corrections and pair propagator for an isotropic s-wave superconductor:[10]

$$\tilde{\eta}_s(\epsilon_n, Q) = \frac{1}{1 - \tilde{\alpha} A_0(\epsilon_n, Q)}, \qquad (12)$$

$$L_s(Q) = \frac{1}{g^{-1} - T\Sigma_n \dfrac{A_0(\epsilon_n, Q)}{1 - \tilde{\alpha} A_0(\epsilon_n, Q)}}. \qquad (13)$$

For dynamical quantities such as the spin-lattice relaxation rate it is necessary to analytically continue the pair propagator from Matsubara energies to the real energy axis. This is done by Eliashberg's technique,[22] leading to the general result

$$L(\omega, q, \phi) = \left\{ N_F \ln\frac{T}{T_c} - \int_0^\infty \frac{d\epsilon}{2\pi}\left[\left(\tanh\frac{\epsilon - \omega/2}{2T} + \tanh\frac{\epsilon + \omega/2}{2T}\right) \operatorname{Im} B_2(\epsilon, q, \phi) - 2\tanh\frac{\epsilon}{2T}\operatorname{Im} B_{2c}(\epsilon) \right] \right.$$

$$\left. + i\int_0^\infty \frac{d\epsilon}{2\pi}\left(\tanh\frac{\epsilon - \omega/2}{2T} - \tanh\frac{\epsilon + \omega/2}{2T}\right)\operatorname{Re} B_2(\epsilon, q, \phi) \right\}^{-1}, \qquad (14)$$

where

$$B_2(\epsilon, q, \phi) = \frac{A_2(\epsilon, q, \phi) + \tilde{\alpha}[A_1^2 - A_2 A_0](\epsilon, q)}{1 - \tilde{\alpha} A_0(\epsilon, q)}, \qquad (15)$$

$$B_{2c}(\epsilon; T) = \frac{T_c}{T} B_2\left(\frac{T_c}{T}\epsilon, \mathbf{q} = 0; T = T_c\right). \qquad (16)$$

Explicit expressions for the functions A_0, A_1, and A_2 are given for s-wave and d-wave pairing in Appendix A.

In the long-wavelength limit it is possible to integrate Eq. (14) analytically and express the pair fluctuation propagator for s-wave or d-wave pairing as

$$L_s(q, \omega) = N_F^{-1} \frac{1}{\epsilon_s + \xi_s^2 q^2 - i\omega\tau_s}, \qquad (17)$$

$$L_d(q, \omega) = N_F^{-1} \frac{1}{\epsilon_d + \xi_d^2 q^2 - i\omega\tau_d}, \qquad (18)$$

where the coherence lengths $\xi_{s,d}$, static pair susceptibilities $\epsilon_{s,d}$, and lifetimes $\tau_{s,d}$ are given in terms of digamma functions of the pair breaking parameters (see Appendix B).[10]

We generalize the pairing fluctuation theory presented above to finite magnetic fields. We assume that the field points along the $\hat{c}$ axis of the crystal, and introduce the following dimensionless field:

$$b = \frac{4|e|B}{\hbar c}\left(\frac{\hbar v_F}{2\pi k_B T_c}\right)^2. \qquad (19)$$

The main effect of the magnetic field is to quantize the orbital motion of the pairs. Through second order in the momentum operator, $\mathbf{q} = -i\nabla - (2e/c)\mathbf{A}$, quantization of the orbital motion is achieved by the replacements[23,18]

$$q^2 \to \left(k + \frac{1}{2}\right)\frac{|b|}{\xi_0^2} \qquad (20)$$

$$\int \frac{d^2q}{(2\pi)^2} \to \frac{|b|}{4\pi\xi_0^2}\sum_{k=0}^\infty, \qquad (21)$$

where $k = 0, 1, \ldots$ labels the different Landau levels.

III. FLUCTUATION CORRECTIONS TO THE NUCLEAR SPIN-LATTICE RELAXATION RATE

The hyperfine interaction between quasiparticles and nuclear spins at (fixed) lattice points $\mathbf{R}_\nu$ is given by

$$\hat{H}_{hf}(\mathbf{R}_\nu) = \gamma_n \gamma_e \hbar^2 \int d^3x \, \hat{\mathbf{I}}(\mathbf{R}_\nu) \underline{a}(\mathbf{x} - \mathbf{R}_\nu) \hat{\mathbf{S}}(\mathbf{x}), \quad (22)$$

where $\hat{\mathbf{I}}$ is the nuclear-spin operator, $\hat{\mathbf{S}}(\mathbf{x})$ is the electron spin-density operator, and $\gamma_{e,n}$ are the gyromagnetic ratios for the electron and nuclear spin, respectively. The coupling of the nuclei to the electronic system occurs via the Hermitian interaction tensor $\underline{a}$, which contains the contact interaction and dipole-dipole interaction between nuclear-spin and electronic-spin density.[21] The nuclear spin-lattice relaxation rate is well described by second-order perturbation theory in the hyperfine interaction between electrons and nuclei. The transition rate $1/{}^\nu T_1^{nn'}$ from nuclear state $|n\rangle$ to $|n'\rangle$ of a nucleus at lattice point $\mathbf{R}_\nu$ is determined by the matrix elements ${}^\nu\mathbf{A}_{pp'}^{nn'}$ for the nuclear transition, accompanied by an electronic transition from state p to p', and by the imaginary part of the electronic dynamical susceptibility:

$$\chi^R_{k\alpha,p\beta,p'\gamma,k'\delta}(\omega) = -\frac{i}{\hbar} \lim_{\delta \to 0} \int_0^\infty dt \, e^{i(\omega + i\delta)t}$$
$$\times \langle [c^+_{k\alpha}(t) c_{p\beta}(t), c^+_{p'\gamma}(0) c_{k'\delta}(0)] \rangle. \quad (23)$$

$c^+_{k\alpha}$ ($c_{k\alpha}$) creates (annihilates) a conduction electron in the Bloch state labeled by k with spin α. We use the shorthand notation $k = (\mathbf{k}, i)$ for a Bloch state with momentum $\mathbf{k}$ in band i. The transition rate is given by

$$\frac{\hbar}{{}^\nu T_1^{nn'}} = 2 k_B T \sum_{kp\alpha\beta} \sum_{k'p'\gamma\delta} ({}^\nu\mathbf{A}_{kp}^{nn'} \boldsymbol{\sigma}_{\alpha\beta})$$
$$\times ({}^\nu\mathbf{A}_{p'k'}^{n'n} \boldsymbol{\sigma}_{\gamma\delta}) \lim_{\omega \to 0} \frac{\mathrm{Im}\, \chi^R_{k\alpha,p\beta,p'\gamma,k'\delta}(\omega)}{\omega}. \quad (24)$$

The matrix elements ${}^\nu\mathbf{A}_{kp}^{nn}$ are smooth functions of the momenta. Hence k and p can be evaluated on the Fermi surface. In terms of Bloch wave functions $\phi_k(\mathbf{x})$ the hyperfine matrix elements are given by

$$^\nu\mathbf{A}_{kp}^{n'n} = \frac{\gamma_n \gamma_e}{2} \hbar^2 \langle n| \hat{\mathbf{I}}(\mathbf{R}_\nu)|n'\rangle \int d^3x \, \phi_k^*(\mathbf{x}) \underline{a}(\mathbf{x} - \mathbf{R}_\nu) \phi_p(\mathbf{x}). \quad (25)$$

and satisfy ${}^\nu\mathbf{A}_{kp}^{nn'} = ({}^\nu\mathbf{A}_{pk}^{n'n})^*$. In what follows we suppress the indices referring to the nuclear transition.

We perform a systematic expansion of $({}^\nu T_1 T)^{-1}$ in the small parameter T_c/E_F (where E_F is the Fermi energy) to
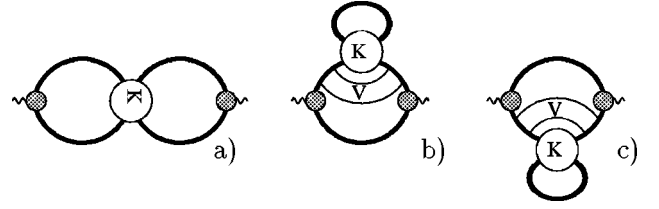

FIG. 2. Leading-order corrections in T_c/E_F to the spin-lattice relaxation rate: (a) Maki-Thompson, (b) and (c) density-of-states corrections. V denotes vertex corrections in the particle-hole channel; $V = 1$ in our model. K denotes the (impurity renormalized) fluctuation mode in the pairing channel, Eq. (9).

obtain the leading-order term of order $(T_c/E_F)^0$, and all corrections of order $(T_c/E_F)^1$ arising from pair fluctuation modes. We neglect pure weak-localization corrections and corrections due to the temperature dependences of the hyperfine coupling matrix elements and of the pairing interaction g. Details of the classification of diagrams in terms of the small parameter T_c/E_F are given in Appendix C. We evaluate the diagrams in Appendix D.

The leading-order contribution to $({}^\nu T_1 T)^{-1}$ is of order $(T_c/E_F)^0$ and defines the Fermi-liquid theory result for the normal-state NSLR rate,

$$({}^\nu T_1 T)_N^{-1} = 4\pi \int d\mathbf{k}_F \int d\mathbf{p}_F N_{\mathbf{k}_F} N_{\mathbf{p}_F} |{}^\nu\mathbf{A}_{\mathbf{k}_F \mathbf{p}_F}|^2, \quad (26)$$

where $N_{\mathbf{k}_F}$ is the angle-resolved quasiparticle density of states on the Fermi surface, and $\mathbf{k}_F$ defines a point on the Fermi surface. The quasiparticle density of states is given by $N_F = \int d\mathbf{k}_F N_{\mathbf{k}_F}$. The right-hand side of Eq. (26) is the Korringa constant.[21]

The fluctuation corrections to $1/T_1 T$ of order T_c/E_F are determined in a diagrammatic expansion of the dynamical susceptibility by the Maki-Thompson (MT) diagram, labeled (a) in Fig. 2, and the two density-of-states (DOS) corrections, labeled (b) and (c) in Fig. 2. The Aslamazov-Larkin diagram (not shown) is another order smaller in the ratio T_c/E_F. The sum of these corrections can be written in the following form:

$$\frac{\delta(T_1 T)^{-1}}{(T_1 T)_N^{-1}} = \frac{T_c}{E_F} \int_0^\infty \frac{v_F^2 q \, dq}{2\pi N_F T_c}$$
$$\times \int_0^{2\pi} \frac{d\phi}{2\pi} [S_M(q,\phi) + S_D(q,\phi)], \quad (27)$$

where the integrand is obtained by analytic continuation (following Eliashberg[22]) of the Maki-Thompson and density-of-states corrections to the dynamical susceptibility obtained from Eqs. (D2) and (D2) of Appendix D:

$$\delta(T_1 T)^{-1} = \lim_{\omega \to 0} 2 \, \mathrm{Im} \frac{\chi_{MT}(\omega) + \chi_{DOS}(\omega)}{\omega}. \quad (28)$$

Thus we obtain for S_D and S_M

$$S_D(q,\phi) = \frac{1}{2} \int_0^\infty \frac{d\omega}{2\pi} \coth \frac{\omega}{2T} \operatorname{Re} L(\omega,q,\phi) \int_0^\infty \frac{d\epsilon}{2\pi} \left[\partial_\epsilon^2 \tanh \frac{\epsilon+\omega/2}{2T} - \partial_\epsilon^2 \tanh \frac{\epsilon-\omega/2}{2T} \right] \operatorname{Re}(B_N B_2(\epsilon,q,\phi))$$

$$+ \frac{1}{2} \int_0^\infty \frac{d\omega}{2\pi} \coth \frac{\omega}{2T} \operatorname{Im} L(\omega,q,\phi) \int_0^\infty \frac{d\epsilon}{2\pi} \left[\partial_\epsilon^2 \tanh \frac{\epsilon+\omega/2}{2T} + \partial_\epsilon^2 \tanh \frac{\epsilon-\omega/2}{2T} \right] \operatorname{Im}(B_N B_2(\epsilon,q,\phi))$$

$$+ \int_0^\infty \frac{d\omega}{2\pi} \left(\partial_\omega \coth \frac{\omega}{2T} \right) \operatorname{Im} L(\omega,q,\phi) \int_0^\infty \frac{d\epsilon}{2\pi} \left[\partial_\epsilon \tanh \frac{\epsilon-\omega/2}{2T} - \partial_\epsilon \tanh \frac{\epsilon+\omega/2}{2T} \right] \operatorname{Im}(B_N B_2(\epsilon,q,\phi)), \quad (29)$$

$$S_M(q,\phi) = -2 \int_0^\infty \frac{d\omega}{2\pi} \coth \frac{\omega}{2T} \operatorname{Re} L(\omega,q,\phi) \int_0^\infty \frac{d\epsilon}{2\pi} \left[\partial_\epsilon \tanh \frac{\epsilon-\omega/2}{2T} - \partial_\epsilon \tanh \frac{\epsilon+\omega/2}{2T} \right] \operatorname{Im}(B_1(\epsilon,q,\phi)^2)$$

$$-2 \int_0^\infty \frac{d\omega}{2\pi} \coth \frac{\omega}{2T} \operatorname{Im} L(\omega,q,\phi) \int_0^\infty \frac{d\epsilon}{2\pi} \left[\partial_\epsilon \tanh \frac{\epsilon-\omega/2}{2T} + \partial_\epsilon \tanh \frac{\epsilon+\omega/2}{2T} \right] \operatorname{Re}(B_1(\epsilon,q,\phi)^2)$$

$$+ 2 \int_0^\infty \frac{d\omega}{2\pi} \left(\partial_\omega \coth \frac{\omega}{2T} \right) \operatorname{Im} L(\omega,q,\phi) \int_0^\infty \frac{d\epsilon}{2\pi} \left[\tanh \frac{\epsilon-\omega/2}{2T} - \tanh \frac{\epsilon+\omega/2}{2T} \right] |B_1(\epsilon,q,\phi)|^2, \quad (30)$$

where $B_N = 2\pi N_F$, $B_2(\epsilon,q,\phi)$ is defined in Eq. (15) and

$$B_1(\epsilon,q,\phi) = \frac{A_1(\epsilon,q,\phi)}{1 - \tilde{\alpha} A_0(\epsilon,q)}. \quad (31)$$

The Fermi energy E_F is related to measurable properties of the 2D Fermi liquid by $E_F = \hbar^2 v_F^2 \pi N_F a_c$, where a_c is the $\hat{c}$-axis dimension of the unit cell. Equation (29) originates from corrections to the rate due to pairing fluctuation corrections to the quasiparticle density of states, Figs. 2(b) and (c). The first two terms in Eq. (29) also determine the fluctuation corrections to the Pauli spin susceptibility, which we discuss in Sec. IV. Equation (30) represents the Maki-Thompson corrections. The first two terms in Eq. (30) are referred to as the ''regular'' Maki-Thompson contribution, and the last term is the ''anomalous'' Maki-Thompson contribution. The regular MT contribution gives a negative correction as does the DOS term. The anomalous MT term is positive, but its magnitude is very sensitive to pair breaking processes. This is the basis for differentiating s-wave and d-wave pairing fluctuations using NMR.

Results for the fluctuation corrections in the quasistatic limit are obtained by expanding the integrand for small ω (the singularities of the coth factors are removable). The long-wavelength limit follows by expanding the denominator of the pair propagator to second order in q and approximating the remaining terms in the integrals by their limits for $q \to 0$. Results for $\delta(1/T_1 T)$ in these limits are discussed by Randeria and Varlamov.[7] We did not make these approximations; rather we performed the ϕ integral analytically and the integrals over ϵ and ω numerically. As we discuss later in this section, our approach is important for extending the theory such that a quantitative comparison with high-field NMR experiments can be made.

In a magnetic field with $H \| \hat{c}$, the orbital motion of the pairing fluctuations is quantized. Landau level quantization is achieved by the replacements shown in Eq. (20). Fluctuation corrections in a magnetic field are often treated in the small field limit, where an expansion in the magnetic field up to second order is performed. At high fields a common ap-

proximation is to retain only the lowest Landau level. However, one is often in the regime between these limits. This is the case for the recent high-field NMR experiments in YBCO.[8,1,2] To analyze this regime we sum the fluctuations over the Landau levels numerically. We introduce a cutoff field b_c to regulate the sum over Landau levels, which would otherwise lead to logarithmically divergent fluctuation corrections. This divergence is an artifact of the (standard) approximation $\xi_{\mathbf{q}-\mathbf{k}} \approx \xi_{\mathbf{k}} - \mathbf{v}_F \cdot \mathbf{q}$ made in evaluating Eq. (4). Without this approximation convergence is achieved on a large momentum scale $\sim k_F$, or correspondingly for n large compared to $1/b$. We simulate the convergence for large n by a cutoff field $b_c = 20$ in our numerical calculations. Thus the sum over the Landau levels in Eq. (20) extends up to b_c/b. Changes in b_c lead only to overall shifts of the results, indicating small field- and temperature-independent ''high-energy'' corrections. These high-energy terms renormalize the leading-order relaxation rate as discussed below.

A. Results: Magnetic field dependence

Calculations of the fluctuation corrections to the NSLR rate are shown in Fig. 3 (for s-wave pairing) and Fig. 4 (for d-wave pairing). We normalized the results by dividing out the small prefactor (T_c/E_f) and the normal-state NSLR rate $(T_1 T)_N^{-1}$; thus we plot the dimensionless quantity $[\delta(T_1 T)^{-1}/(T_1 T)_N^{-1}](E_F/T_c)$. Pairing fluctuation corrections in two dimensions contain contributions that are constant in temperature and magnetic field. The exact values of these constants are weakly dependent on the cutoff in the Landau-level summation as mentioned above. These constants, which appear as offsets of the curves in all following figures, are irrelevant and simply renormalize the normal-state rate $(T_1 T)_N^{-1}$.

Our calculations for the fluctuation corrections to $1/T_1 T$ for s-wave and d-wave pairing symmetry include pairbreaking processes from elastic electron-impurity scattering and inelastic scattering by emission and absorption of phonons. For s-wave symmetry we fixed the elastic scattering rate at $\alpha = 0.2$, and plotted the corrections for the pair breaking pa-
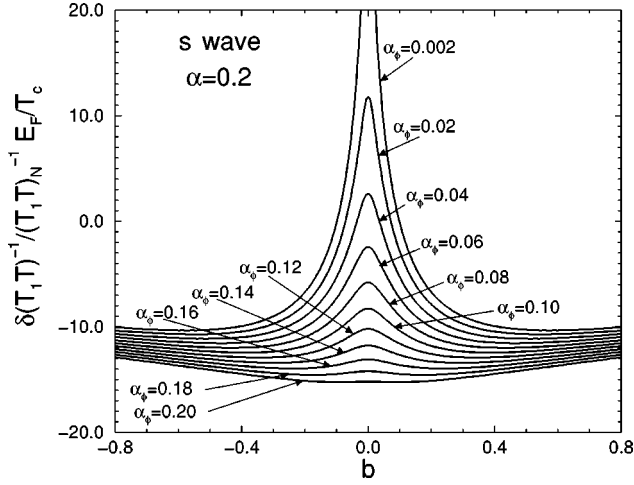
FIG. 3. Corrections to the spin-lattice relaxation rate for $T/T_c = 95\,\text{K}/92.5\,\text{K} \approx 1.03$ from s-wave pairing fluctuations as a function of the reduced magnetic field b. The elastic-scattering parameter is $\alpha = 0.2$, and the pair breaking parameter α_ϕ varies as indicated.

rameter α_ϕ ranging from 0.002 to 0.2. However, for d-wave symmetry nonmagnetic impurities are already pair breaking, so we fixed $\alpha_\phi = 0.001$ (this value affects the results only in the ultraclean case) and calculated the fluctuation corrections for impurity scattering rates ranging from $\alpha = 0.002$ to 0.2. Our results are shown in Figs. 3 and 4. Note that the lowest curve in the d-wave case (Fig. 4) and the highest curve in the s-wave case (Fig. 3) correspond to similar impurity and inelastic scattering rates, and that s-wave and d-wave pairing fluctuations show the opposite field evolution in the limit $\alpha_\phi \ll \alpha \approx 0.2$. Furthermore, the s-wave fluctuation corrections to the NSLR rate decrease with increasing field even for inelastic rates as large as $\alpha_\phi \approx 0.1$. For very large inelastic rates, $\alpha_\phi \gtrsim 0.2$, the maximum in $\delta(T_1 T)^{-1}$ at $b = 0$ is suppressed. Such a large inelastic pairbreaking parameter appears unlikely for the cuprates. More realistic estimates for the elastic and inelastic pairbreaking parameters are $\alpha_\phi \approx 0.02$ and $\alpha \approx 0.2$.[17,18]
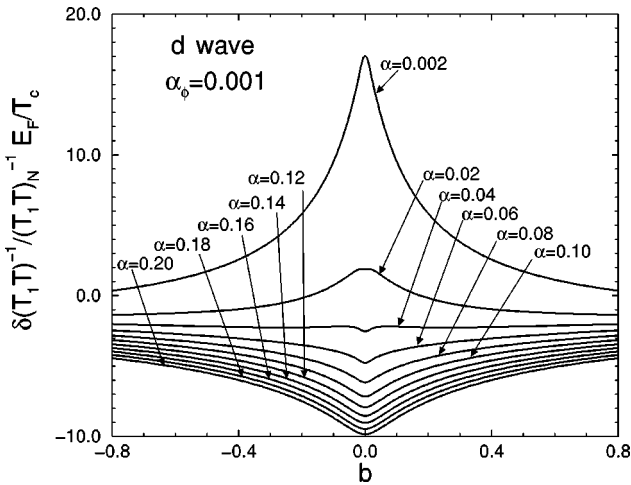

FIG. 4. Corrections to the spin-lattice relaxation rate for $T/T_c = 95\,\text{K}/92.5\,\text{K} \approx 1.03$ from d-wave pairing fluctuations as a function of the reduced magnetic field b. The pair breaking parameter is $\alpha_\phi = 0.001$ and the elastic-scattering parameter α varies as indicated.
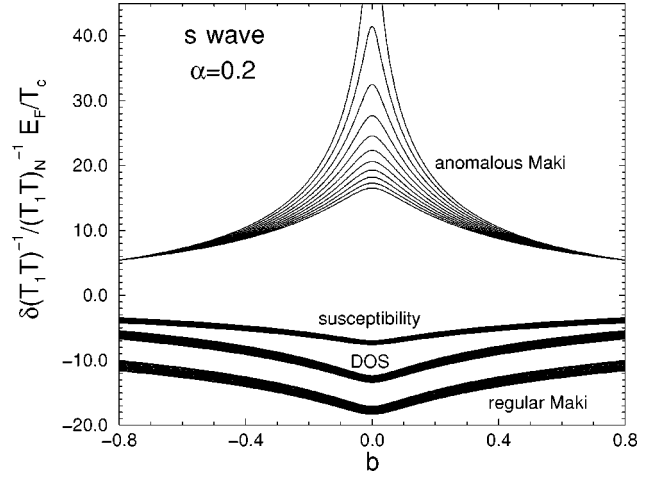

FIG. 5. Magnetic-field dependence of the Maki-Thompson contributions and the DOS contribution to the fluctuation corrections to the NSLR rate for $T/T_c = 95\,\text{K}/92.5\,\text{K} \approx 1.03$, assuming s-wave pairing. For comparison, we also show the fluctuation corrections to the Pauli spin susceptibility. The curves correspond to $\alpha_\phi = 0.002$ and $\alpha_\phi = 0.02-0.2$ (in steps of 0.02) from top to bottom for each set.

For d-wave pairing the fluctuation correction to the NSLR rate changes sign for $\alpha \approx 0.03$; the rate decreases with increasing field in the ultraclean limit and increases with increasing field in the limit of weak disorder, $\alpha > 0.03$. In Fig. 4 we note the rapid drop in the rate with increasing field in the ultraclean limit ($\alpha = 0.002$) compared with the increase in the rate with increasing field shown for $\alpha = 0.2$. It is worth noting that this behavior is not obtained in the long-wavelength approximation employed by other authors.[10] We also note that in the clean limit for d-wave pairing the long-wavelength approximation is not justified for $(T - T_c)/T_c \gtrsim (\alpha + \alpha_\phi)$.[24]

In Figs. 5 and 6 we show the different contributions to the relaxation rate for s-wave and d-wave symmetries. The label ''DOS'' refers to the density-of-states corrections in Eq. (29). The ''regular Maki'' contribution is the first two terms
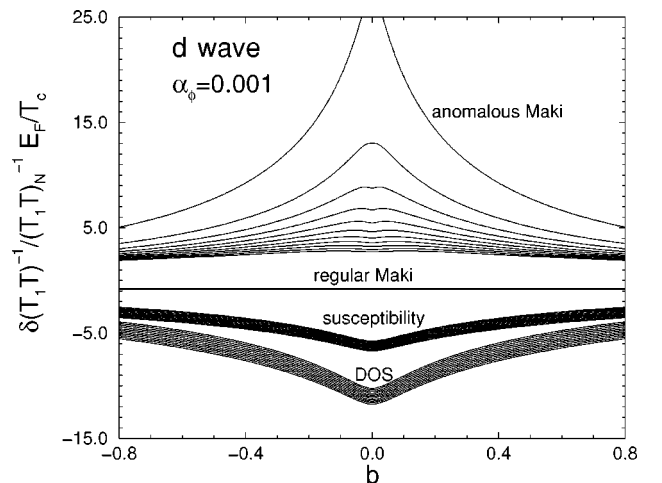

FIG. 6. The same as in Fig. 5, but for d-wave pairing; $\alpha = 0.002$ and $\alpha = 0.02-0.2$ (in steps of 0.02) from top to bottom for each set. Note that the anomalous Maki-Thompson term dominates for very clean systems, $\alpha \lesssim 0.04$, but is negligible for $\alpha \gtrsim 0.1$.
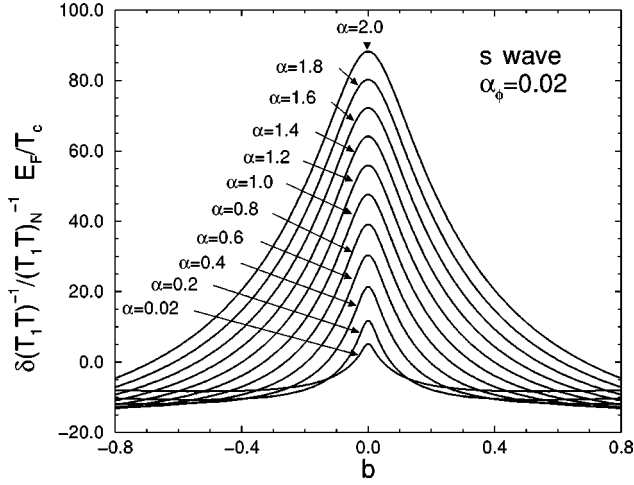
FIG. 7. Fluctuation corrections to NSLR rate for $T/T_c = 95$ K/92.5 K ≈ 1.03 for α ranging from the clean to the dirty limit.

FIG. 8. Upper critical field b_{c2} for α ranging from the clean to the dirty limit.

in Eq. (30) and the ''anomalous Maki'' correction corresponds to the last term in Eq. (30). The full fluctuation correction to $\delta(T_1T)^{-1}$, shown in Figs. 3 and 4, is the sum of the DOS, regular Maki, and anomalous Maki corrections. The DOS term also determines the fluctuation correction to the tunneling density of states at zero bias for a normal metal–insulator–superconductor tunnel junction. The fluctuation corrections to the spin susceptibility are also shown for comparison in Figs. 5 and 6.

For s-wave pairing the regular Maki-Thompson correction is (up to a constant) nearly equal to the DOS contribution. By contrast, the regular Maki-Thompson term is negligible for d-wave pairing. All fluctuation corrections except the anomalous Maki-Thompson term are weakly dependent on the scattering parameters in the range of interest. The anomalous Maki-Thompson correction is extremely sensitive to pair breaking, as can be seen in Figs. 5 and 6. Because pair breaking by disorder is sensitive to the symmetry of the pairing fluctuations, the relative correction to the NSLR rate, shown in Figs. 3 and 4, shows qualitatively different behavior for s-wave and d-wave pairing symmetries.

In Fig. 7 we show the influence of strong disorder on the magnetic-field dependence of the NSLR rate for an s-wave superconductor. Disorder leads to a reduction of the coherence length, and thus to an enhancement of fluctuations. In the clean limit the typical magnitude of the fluctuation corrections in 2D contains the prefactor T_c/E_F which is replaced in the dirty limit ($\alpha = 1/2\pi\tau T_c \gg 1$) by $1/\tau E_F \sim \alpha T_c/E_F$, which means that the fluctuations in dirty s-wave superconductors are typically stronger than fluctuations in clean s-wave superconductors with the same T_c. By comparison, d-wave superconductivity is completely suppressed by elastic scattering for $1/2\pi\tau T_{c0} \gtrsim 0.28$, where T_{c0} is the transition temperature without impurities.

Note that the NSLR rate for s-wave pairing decreases with increasing field in both the clean and dirty limit for realistic pair breaking parameters $\alpha_\phi \lesssim 0.2$. The enhancement of fluctuation corrections to the rate reflects the reduction in the coherence length by elastic and inelastic scattering. For weak impurity scattering the reduction of the coherence length at T_c for s-wave pairing becomes
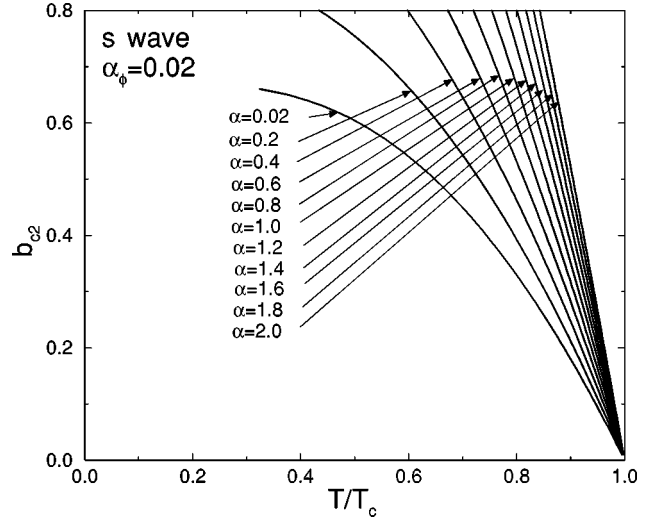
$$\frac{\xi_s(T_c)^2}{\xi_0(T_c)^2} = a - \frac{\pi^4}{32}\left(\alpha_\phi + \frac{\alpha}{3}\right), \tag{32}$$

and for d-wave pairing

$$\frac{\xi_d(T_c)^2}{\xi_0(T_c)^2} = a - \frac{\pi^4}{32}(\alpha_\phi + \alpha), \tag{33}$$

where $a = 7\zeta(3)/8 \approx 1.05$. Thus the reduction of the coherence length by nonmagnetic impurities is stronger by a factor of 3 for d-wave pairing compared to s-wave pairing at the same T_c. This shortening of the coherence length is accompanied by a suppression of the transition from $T_{c0} = T_c[1 + \pi^2/4(\alpha_\phi + \alpha)]$ to T_c in d-wave symmetry, compared to $T_{c0} = T_c(1 + \pi^2/4\alpha_\phi)$ for s-wave pairing.[15,16]

The slope of b_{c2} at T_c is inversely proportional to the square of the coherence length,

$$\left.\frac{db_{c2,s(d)}}{dT}\right|_{T=T_c} = -2\frac{\xi_0^2}{\xi_{s(d)}^2}\left.\frac{d\epsilon_{s(d)}}{dT}\right|_{T=T_c}. \tag{34}$$

Thus the reduction in the coherence length leads to a significant increase in the slope of $b_{c2}(T)$ shown in Fig. 8. These results were obtained by numerically solving the equation

$$\ln\frac{T}{T_c} = N_F^{-1}\int_0^\infty \frac{d\epsilon}{2\pi}2\tanh\frac{\epsilon}{2T}\text{Im}[B_2(\epsilon, q_b; T) - B_{2c}(\epsilon; T)], \tag{35}$$

where $q_b = \sqrt{|b_{c2}(T)|/2\xi_0^2}$.[25]

For weak impurity scattering we obtain

$$\left.\frac{db_{c2}}{dT}\right|_{T_c} = -\frac{2}{aT_c}\left(1 - \frac{\pi^2\alpha_\phi}{4} + \frac{\pi^4}{32a}\left(\alpha_\phi + \frac{\alpha}{3}\right)\right) \tag{36}$$

$$\approx -\frac{1}{T_c}(1.90 + 0.81\alpha_\phi + 1.83\alpha), \tag{37}$$

for s-wave pairing, and

$$\left.\frac{db_{c2}}{dT}\right|_{T_c} = -\frac{2}{aT_c}\left(1 - \frac{\pi^2(\alpha + \alpha_\phi)}{4} + \frac{\pi^4}{32a}(\alpha_\phi + \alpha)\right) \tag{38}$$
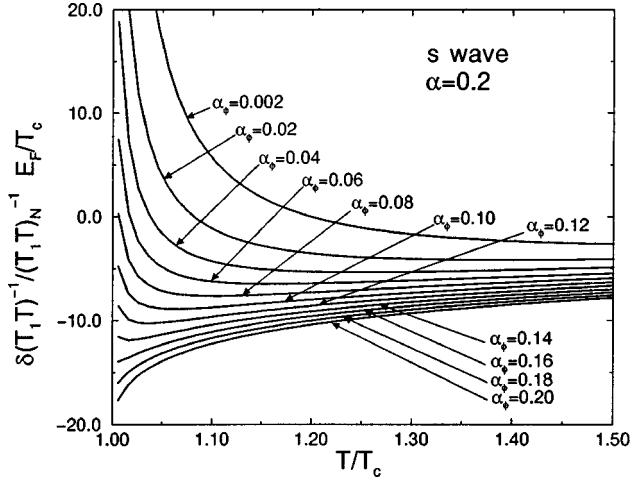
FIG. 9. Temperature dependence of fluctuation corrections to NSLR rate for $b=0.01$, $\alpha=0.2$, and s-wave pairing.

$$\approx -\frac{1}{T_c}(1.90+0.81\alpha_\phi+0.81\alpha), \qquad (39)$$

for d-wave pairing. The negative terms in the brackets come from the reduction of the transition temperature by pair breaking.

B. Results: Temperature dependence

The theory of leading-order pairing fluctuations predicts characteristic features in the temperature dependence of the fluctuation corrections to the NSLR rate $1/T_1$. Typical results for s-wave and d-wave pairing are shown in Figs. 9–16. For both symmetries there is a pronounced enhancement of the absolute value of the fluctuation corrections when the mean-field transition temperature $T_c(b)$ is approached. However, depending on the scattering parameters α and α_ϕ, the corrections may be positive or negative near $T_c(b)$.

We first show in Figs. 9–12 the influence of impurities on $1/T_1$ for small and intermediate values of the magnetic field $b=0.01$ and $b=0.4$. For s-wave symmetry we show results for fixed elastic scattering $\alpha=0.2$, for a range of pair break-
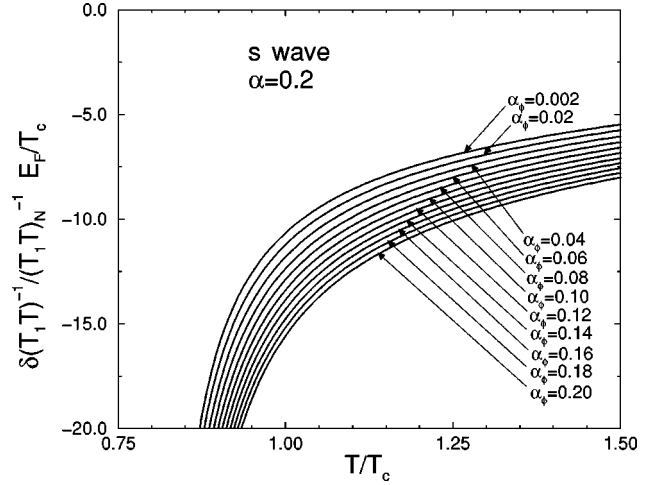

FIG. 11. Temperature dependence of fluctuation corrections to NSLR rate for $b=0.4$, $\alpha=0.2$, and s-wave pairing.

ing parameters α_ϕ. In the low-field limit, shown in Fig. 9, a crossover from positive to negative divergence takes place for $\alpha_\phi\approx 0.16$. The divergence is much weaker for strong pair breaking compared to weak pair breaking in the relatively clean case of $\alpha\lesssim 0.2$ discussed in this paper. Note that in the clean limit the correction to $1/T_1$ diverges like $\sqrt{T_c/(T-T_c)}$ in zero field,[7] compared to a logarithmic divergence in the dirty case.[5] In the dirty limit the crossover from a positive logarithmic divergence to a negative logarithmic divergence takes place at $\alpha_\phi\approx 0.26$.[20] The low-field results for d-wave symmetry are shown in Fig. 10. Because inelastic and elastic scattering act similarly in d-wave superconductors we fixed $\alpha_\phi=0.001$ and present results for several values of the elastic-scattering rate α. As can be seen in Fig. 10 there is a crossover from a positive to a negative divergence for $\alpha\approx 0.04$, corresponding to a mean free path of about 25 coherence lengths. For realistic values of scattering parameters in high-T_c superconductors, $\alpha+\alpha_\phi\approx 0.2$, a negative divergence should be observed.

The effects of a strong field, $b=0.4$, are shown in Figs. 11 and 12. For s-wave fluctuations the pair breaking effect of the magnetic field dominates the effect of intrinsic pair
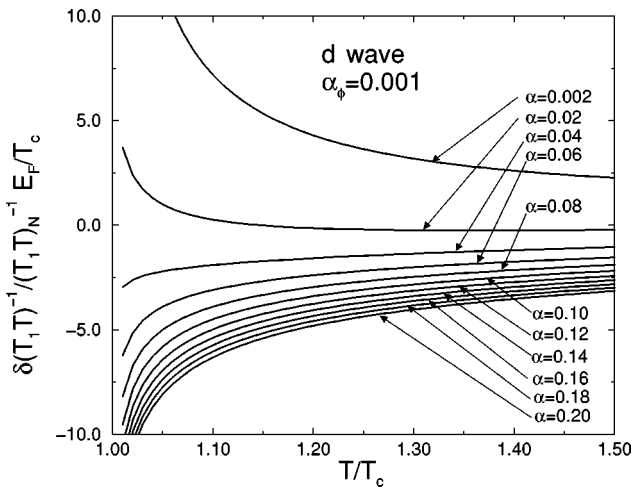

FIG. 10. Temperature dependence of fluctuation corrections to NSLR rate for $b=0.01$, $\alpha_\phi=0.001$, and d-wave pairing.
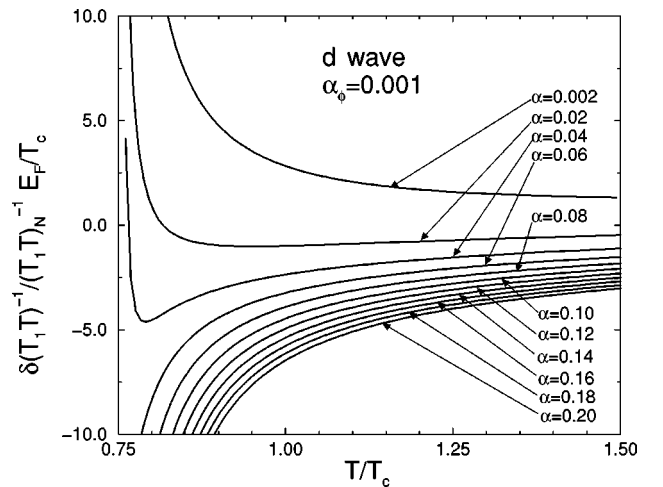

FIG. 12. Temperature dependence of fluctuation corrections to NSLR rate for $b=0.4$, $\alpha_\phi=0.001$, and d-wave pairing.
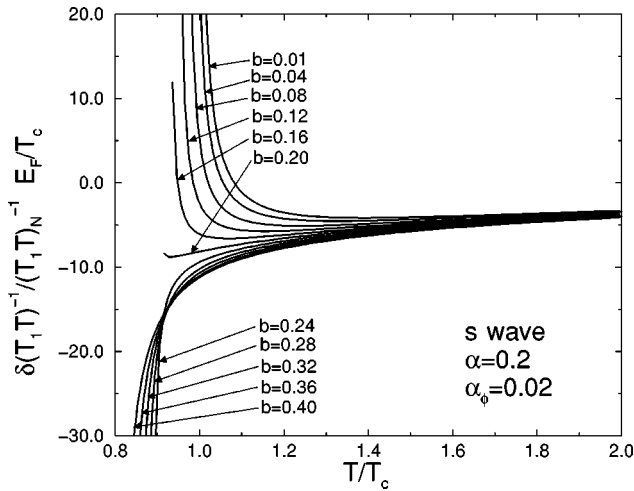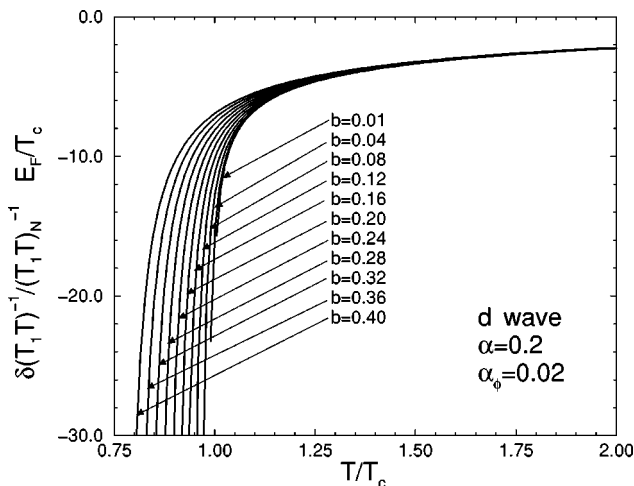
FIG. 13. Temperature dependence of s-wave fluctuation corrections to NSLR rate for different fields, given as the sum of anomalous Maki, regular Maki, and DOS terms.

breaking, leading to large negative fluctuation corrections to the NSLR rate as shown in Fig. 11. For d-wave pairing the effect of a magnetic field is much less pronounced. In the clean limit, even at high magnetic fields, the fluctuation contributions to the NSLR rate show a positive divergence for d-wave pairing, in sharp contrast to s-wave pairing. We discuss this result in more detail below. However, for cuprate superconductors with d-wave pairing, and a reasonable estimate for the scattering rate $\alpha \approx 0.2$, we obtain a negative correction for all field strengths.

As can be seen by comparison of the NSLR rate for $b = 0.01$ and $b = 0.4$, there is a strong effect of the magnetic field on the temperature dependence in s-wave superconductors. The temperature dependences of the NSLR rate of superconductors with s- and d-wave pairing are compared in Figs. 13 and 14 for different magnetic field strengths and parameters $\alpha = 0.2$, $\alpha_\phi = 0.02$, which are typical estimates for high-T_c superconductors.[17]

In Fig. 13 we show, for s-wave pairing, that there is a dramatic change in the behavior of the corrections to the

NSLR rate at field $b \approx 0.2$ for T near $T_c(b)$. Whereas for $b \lesssim 0.2$ fluctuations *enhance* the NSLR rate with decreasing temperature, for $b \gtrsim 0.2$ fluctuations *suppress* the NSLR rate with decreasing temperature. Note that to observe this effect one must compare the qualitative temperature behavior of the NSLR rate for different fields rather than changing the magnetic field at constant temperature. For d-wave symmetry, shown in Fig. 14, this effect is absent.

To clarify the origin of this behavior we have plotted the Maki-Thompson terms and the DOS term separately in Figs. 15 and 16. As can be seen, all contributions to the fluctuations are reduced in magnitude at constant temperature with increasing magnetic field. In contrast, all terms are enhanced in magnitude with increasing magnetic field for constant $T - T_c(b)$, as can be inferred from the larger slope of $\delta(T_1 T)^{-1}$ near $T_c(b)$ at lower fields.
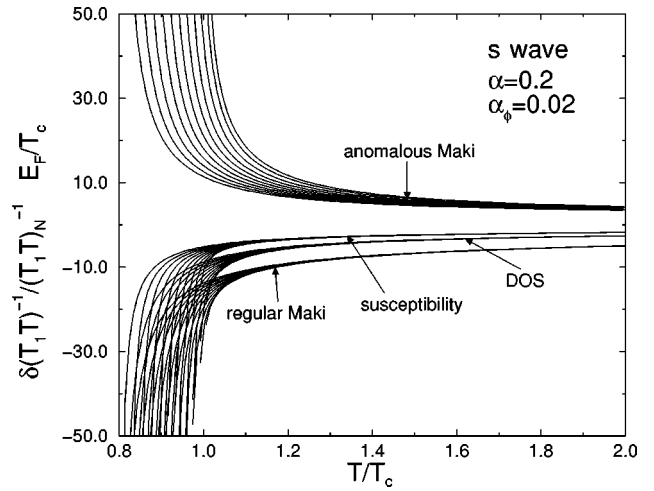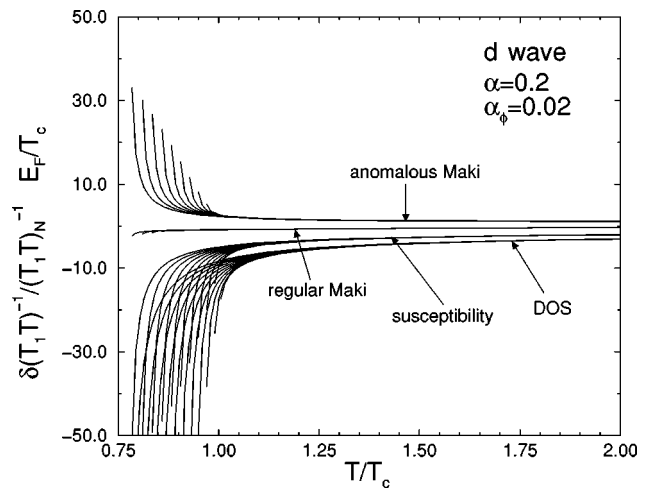

FIG. 15. Temperature dependence of the Maki-Thompson contributions and the DOS contribution to the fluctuation corrections in the NSLR rate, assuming s-wave pairing. The curves are shown for different fields, ranging from 0.01, 0.04–0.4 (in steps of 0.04), from right to left. For comparison, we also show the fluctuation corrections to the Pauli spin susceptibility.

FIG. 14. Temperature dependence of d-wave fluctuation corrections to NSLR rate for different fields, given as the sum of anomalous Maki, regular Maki, and DOS terms.

FIG. 16. The same as in Fig. 15, for d-wave pairing. Note that the regular Maki-Thompson term is negligible compared to the other terms at all temperatures. The anomalous Maki-Thompson term is negligible at $b = 0$ for $\alpha = 0.2$ and $\alpha_\phi = 0.02$, but contributes considerably at higher fields, $b \gtrsim 0.2$.

Neither the DOS nor the regular Maki-Thompson correction alone are large enough to dominate the anomalous Maki-Thompson contribution. But together these two corrections overcompensate the anomalous MT correction for fields above $b \gtrsim 0.2$ for s-wave pairing, which leads to the qualitative changes shown in Fig. 13. In d-wave pairing the regular MT contribution is negligible for all magnetic-field strengths, as shown in Fig. 16. This is true also for the regular MT contribution in the ultraclean limit, not shown here, and explains why there is no change in sign of fluctuation corrections with increasing magnetic field for d-wave pairing. We also show for d-wave pairing in Fig. 16 that the anomalous Maki-Thompson term cannot be neglected near T_c; it diverges at the mean-field transition temperature $T_c(b)$, except for zero magnetic field b.

Finally, we suggest that the change in sign of the fluctuation corrections to the NSLR rate for s-wave pairing with increasing field should be observable in the electron doped compounds like $Nd_{2-x}Ce_xCuO_{4-\delta}$, if they have s-wave pairing symmetry. Observation of this effect would be a strong confirmation of s-wave pairing in these compounds.

C. Comparison with experiment

In order to compare our results with experimental results obtained in high-T_c cuprate superconductors, we discuss first some specific aspects of NMR in these compounds. In addition to superconducting fluctuations antiferromagnetic spin fluctuations are believed to play an important role in the cuprates.[26] A spin pseudogap may occur at the antiferromagnetic wave vectors $\mathbf{q} = \mathbf{Q}_{AF}$, which manifests itself in the temperature dependence of the NSLR rate of the Cu(2) nuclear spins. The NSLR rate is proportional to the slope at zero energy of the dynamical susceptibility at the positions of the nuclei, i.e., $\lim_{\omega \to 0} \chi''(\mathbf{R}_\nu, \omega)/\omega$, and is especially sensitive to changes in the spectral weight of low-energy electronic excitations. On the other hand, the Knight-shift tensor, which probes the static spin susceptibility at $\mathbf{q} = 0$, is barely affected by the opening of the antiferromagnetic spin pseudogap at $\mathbf{Q}_{AF}$. By contrast the opening of a pairing pseudogap at $\mathbf{q} = 0$ affects the quasiparticle density of states at the Fermi level N_F and thus both the nuclear spin-lattice relaxation rate $(\sim N_F^2)$ and the Knight shift $(\sim N_F)$.

Recent experiments by Mitrović $et\ al.$[1] and Bachman $et\ al.$[2] reported the characteristic field scale on which the pseudogap behavior is suppressed, $H^* \approx 10$ T in optimally doped YBCO. Assuming that antiferromagnetic correlations lead to a suppression of spectral weight on the scale $J \sim 100$ meV, corresponding to $J/\mu_B \sim 1700$ T, this comparatively low magnetic-field scale has to be assigned to another origin. Similarly, recent neutron-scattering experiments in fully oxygenated YBCO show that the spin-fluctuation spectrum near the antiferromagnetic wave vector remains almost unaffected by a field of 11.5 T.[27] However, if spin fluctuations are responsible for the pairing interaction between quasiparticles, it is possible that strong coupling between quasiparticles and spin fluctuations may lead to a pseudogap which has characteristics of both spin fluctuations and pairing fluctuations. At present a strong-coupling theory of su-
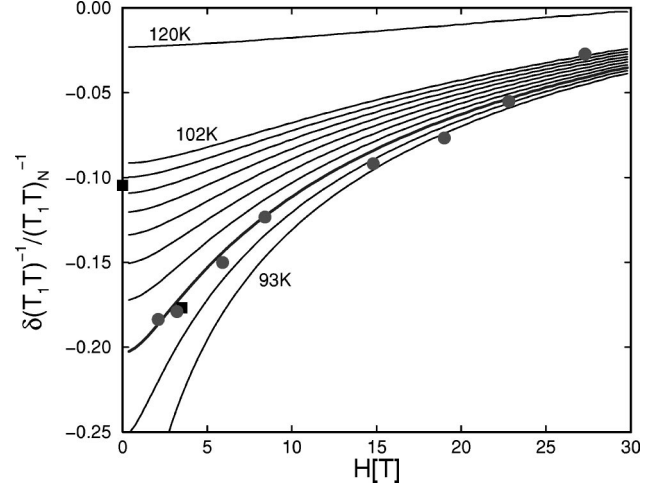

FIG. 17. d-wave calculations for the superconducting pairing fluctuation contribution $\delta(T_1T)^{-1}/(T_1T)_N^{-1}$ of $^{63}Cu(2)$ spin-lattice relaxation rate in optimally doped YBCO as a function of magnetic field at temperatures ranging from 93 to 102 K in increments of 1 K, and for 120 K. Circles[1] and squares[28] are NMR and NQR (0 T) experiments. The thick curve and the experimental data correspond to 95 K.

perconducting fluctuations and antiferromagnetic spin fluctuations has not been developed for pseudogap behavior in high magnetic fields.

Our results are based on the theory of weak-coupling 2D pairing fluctuations. Two-dimensional fluctuation theory for YBCO is justified in the presence of magnetic fields because of the large vortex liquid region below the transition. Phase coherence between planes may be neglected in the vortex liquid state because of rapid thermal motion of the pancake vortices. Thus it is reasonable to neglect the Josephson coupling in the crossover region from the normal to vortex liquid state as well. This fact, and Landau level quantization in strong magnetic fields, implies that fluctuations are predominantly two-dimensional. It is possible that for fields smaller than 2 T a crossover to three-dimensional behavior might occur close to T_c.

We compare our calculations with experiments recently reported by Mitrović $et\ al.$[1] on optimally doped $YBa_2Cu_3O_{6.95}$ in a magnetic field $H \| \hat{c}$. Our calculations, which assume two-dimensional, d-wave pairing fluctuations describe the experimental NMR data remarkably well. The relative fluctuation correction $\delta(T_1T)^{-1}/(T_1T)_N^{-1}$ to $1/T_1T$ for d-wave pairing and $\alpha = 0.2$ and several temperatures is shown in Fig. 17. We define the normal-state rate $(T_1T)_N^{-1}$ to include pairing fluctuation corrections that are constant in temperature and magnetic field. Thus to compare with experiments we subtract these constant shifts from the calculated fluctuation corrections as discussed in Sec. III A, and define $\delta(T_1T)^{-1} \equiv (T_1T)^{-1} - (T_1T)_N^{-1}$. We chose the value of the rate at 120 K and 30 T for this subtraction. The experimental results from Mitrović $et\ al.$[1] for the fluctuation correction are also shown for the temperature $T = 95$ K. In order to compare theory and experiment we subtracted from the experimental data the asymptotic normal-state rate, which is well described by $(T_1T)_N^{-1} \sim T_x/(T + T_x)$, to extract the fluctuation correction $\delta(T_1T)^{-1}$.

The zero-field transition temperature of $T_c(0) = 92.5 \, \text{K}$ determines the absolute temperature scale for the theoretical calculations. We solve numerically Eq. (35) for the reduction of the mean-field transition temperature as a result of Landau quantization. Theoretically the mean-field transition temperature is determined by diverging pairing fluctuations. To fix the magnetic-field scale we use the value for the mean-field transition temperature at 8.4 T obtained from our fit to the fluctuation corrections to the Pauli spin susceptibility,[2] discussed in Sec. IV. There is one fitting parameter, T_c/E_F, which scales the magnitude of the fluctuation contributions. As shown in Fig. 17, the agreement between the d-wave fluctuation theory and the experimental data from Ref. 1 is excellent.

We also show in Fig. 17 data from Y.-Q. Song (black squares).[28] The data point at $H = 0$ is the NQR rate. The NQR rate is *higher* than the low-field NMR rate in the same sample at 3.5 T. A similar drop between the NQR rate and the low-field NMR rate was obtained by Carretta et al. on optimally doped YBCO.[8] Based on the larger NQR rate compared with the NMR rate at 5.9 T, Carretta et al. concluded that fluctuation corrections to the NSLR rate are predominantly s-wave.[8] However, the field evolution of the NSLR rate from 2 to 27 T is in quantitative agreement with the theory of 2D pairing fluctuations with d-wave symmetry, and disagrees qualitatively and quantitatively with the theory of s-wave fluctuations. The apparent discrepancy between the NQR rate and the low-field NMR rate requires explanation. We propose an explanation for the low-field evolution ($0 \leq H \lesssim 2$ T) that reconciles Carretta et al.'s suggestion in terms of s-wave pairing fluctuations with the field evolution and our explanation in terms of d-wave pairing fluctuations. We show below that subdominant s-wave fluctuations, induced by the orthorhombic anisotropy of YBCO, can account for the low-field evolution. At fields, $H \gtrsim 2$ T the s-wave fluctuations are suppressed and the dominant d-wave fluctuations control the field evolution.

D. Effect of orthorhombic distortion

If the crystal symmetry is not perfectly tetragonal, then the s-wave and d-wave pairing channels correspond to the same irreducible representation. Thus the pairing basis function $\eta(\psi)$ is of the form

$$\eta(\psi) = \beta_s \eta_s(\psi) + \beta_d \eta_d(\psi) \qquad (40)$$

with $\beta_s^2 + \beta_d^2 = 1$. The results obtained for the fluctuation formulas for pure s- and d-wave pairing, Eqs. (27)–(30), are the same with the replacements

$$B_1(\epsilon, q, \phi) = \beta_d \frac{A_1(\epsilon, q, \phi)}{1 - \tilde{\alpha} A_0(\epsilon, q)} + \beta_s \frac{A_0(\epsilon, q, \phi)}{1 - \tilde{\alpha} A_0(\epsilon, q)},$$

$$(41)$$

$$B_2(\epsilon, q, \phi) = \beta_d^2 \frac{A_2(\epsilon, q, \phi) + \tilde{\alpha}[A_1^2 - A_2 A_0](\epsilon, q)}{1 - \tilde{\alpha} A_0(\epsilon, q)}$$

$$+ \beta_s^2 \frac{A_0(\epsilon, q, \phi)}{1 - \tilde{\alpha} A_0(\epsilon, q)} + 2\beta_s \beta_d \frac{A_1(\epsilon, q, \phi)}{1 - \tilde{\alpha} A_0(\epsilon, q)}.$$
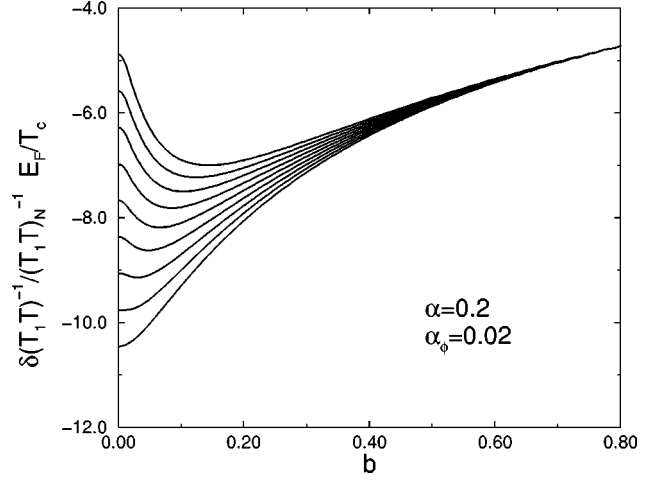
$$(42)$$

FIG. 18. Fluctuation corrections to nuclear spin-relaxation rate taking into account orthorhombic distortion. We assumed an induced asymmetry in the order parameter described by $\eta(\psi) = \beta_d \eta_d(\psi) + \beta_s \eta_s$, with β_s^2 varying from 0 to 0.2 in steps of 0.025 from bottom to top, and $\beta_d^2 = 1 - \beta_s^2$.

Because $A_1 \sim \cos 2\phi$ the mixed terms in B_2 and B_1^2 which enter in the Eqs. (29) and (30) are canceled to a large extent by averaging over ϕ. So near T_c it is a good approximation to add the s- and d-wave components of the fluctuation corrections with weights β_s^2 and β_d^2, respectively.

In Fig. 18 we show the result for $\delta(T_1 T)^{-1}$ with β_s^2 ranging from 0 to 0.2. Thus the low-field anomaly in the experimental data of Fig. 17 can be accounted for by a small s-wave component induced by an orthorhombic distortion, as can be seen comparing with Fig. 18. We estimate $\beta_s^2 \approx 0.15$ ($\beta_d^2 \approx 0.85$) for optimally doped YBCO. Note that $b = 0.8$ corresponds to $H = 29$ T and that we account for both the position of the minimum in the NMR rate (at ≈ 2 T) and the difference between NQR and low-field NMR rates with one fitting parameter (β_s).

In BSCCO this effect should be absent if the dominant pairing channel has B_{1g} symmetry ($d_{x^2-y^2}$), because in this case the lattice distortion does not induce an s-wave, but rather a g-wave component with A_{2g} symmetry, which has fluctuation corrections that respond to disorder and field similarly to the d-wave component. However, an s-wave component would be induced if the order parameter of BSCCO is predominantly B_{2g}-symmetry (d_{xy}).

IV. FLUCTUATION CORRECTIONS TO THE PAULI SPIN SUSCEPTIBILITY

The Pauli spin susceptibility is obtained from the long-wavelength limit of the particle-hole susceptibility at $\omega_e = 0$:

$$\chi_s = \mu_e^2 \sum_{k\alpha\beta} \sum_{p\gamma\delta} (\boldsymbol{\sigma}_{\alpha\beta} \cdot \hat{\mathbf{h}})(\boldsymbol{\sigma}_{\gamma\delta} \cdot \hat{\mathbf{h}}) \chi^R_{p\gamma, p\,\delta, k\alpha, k\beta}(\omega_e = 0),$$

$$(43)$$

where $\hat{\mathbf{h}}$ is a unit vector in direction of the applied field and $\mu_e = \gamma_e \hbar/2$. The Pauli spin susceptibility can be obtained from the spin part of the measured NMR Knight shift by subtraction of the orbital and diamagnetic contributions. As-

suming an isotropic hyperfine matrix element $^\nu A_{kk}$ and neglecting anisotropic band structure and exchange interaction, the spin shift K_{spin} is directly proportional to the Pauli spin susceptibility χ_s. The zeroth-order terms in T_c/E_F for the particle-hole response function (at $\omega_e=0$) define the Fermi-liquid result for the Pauli spin susceptibility χ_N.

The spin susceptibility can be obtained directly from the Matsubara Green's functions without analytic continuation because it is an equilibrium quantity. Nevertheless, it is instructive to write down the expression for $\delta\chi$ in terms of retarded and advanced Green's functions defined on the real energy axis.

The pairing fluctuation corrections to leading order in T_c/E_F for the static ($\omega_e=0$) long-wavelength ($q_e\rightarrow 0$) spin susceptibility are obtained by the procedure discussed in Appendix C, and are summarized by the DOS, Maki-Thompson, and Aslamazov-Larkin diagrams, shown in Fig. 19.[29] Note that in contrast to the large-q_e response the contribution ''d'' in Fig. 19 has the same order in T_c/E_F as the DOS and MT contributions. However, it contains only one singlet pair fluctuation mode, the other mode in the particle-particle channel is a triplet impurity Cooperon mode. Algebraic expressions for these diagrams are given in Appendix
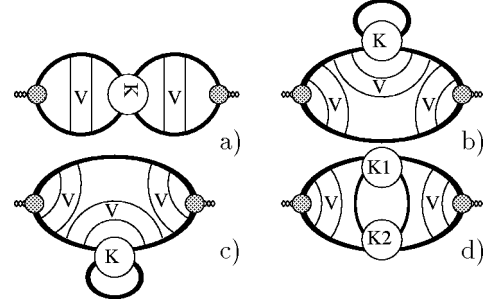

FIG. 19. First corrections in T_c/E_F to the Pauli spin susceptibility. V denotes vertex corrections in the particle-hole channel; $V=1$ in our model. K, $K1$, and $K2$ denote the (impurity renormalized) fluctuation modes in the pairing channel. For the Pauli spin susceptibility $K1$ and $K2$ either are a singlet Cooperon or a triplet impurity Cooperon in a complementary way.

D. The sum of the leading order corrections in Eq. (D28) of App. D leads to the following expression for the relative fluctuation contribution to the Pauli spin susceptibility:

$$\frac{\delta\chi}{\chi_N}=\frac{T_c}{E_F}\int_0^\infty \frac{v_F^2 q\,dq}{2\pi T_c}\int_0^{2\pi}\frac{d\phi}{2\pi}S(q,\phi),\qquad (44)$$

where $S(q,\phi)$ sums the contributions from all diagrams shown in Fig. 19 and is given by

$$S(q,\phi)=\pi\int_0^\infty \frac{d\omega}{2\pi}\coth\frac{\omega}{2T}\operatorname{Re}L(\omega,q,\phi)\int_0^\infty \frac{d\epsilon}{2\pi}\left[\partial_\epsilon^2\tanh\frac{\epsilon+\omega/2}{2T}-\partial_\epsilon^2\tanh\frac{\epsilon-\omega/2}{2T}\right]\operatorname{Re}B_2(\epsilon,q,\phi)$$

$$+\pi\int_0^\infty \frac{d\omega}{2\pi}\coth\frac{\omega}{2T}\operatorname{Im}L(\omega,q,\phi)\int_0^\infty \frac{d\epsilon}{2\pi}\left[\partial_\epsilon^2\tanh\frac{\epsilon+\omega/2}{2T}+\partial_\epsilon^2\tanh\frac{\epsilon-\omega/2}{2T}\right]\operatorname{Im}B_2(\epsilon,q,\phi).\qquad (45)$$

Comparing with Eq. (29) one realizes that the fluctuation correction to the Pauli spin susceptibility is given exactly by the first two lines of the density-of-states contribution to the NSLR rate in Eq. (29). This result is nontrivial not only because the fluctuation corrections to the NSLR rate and spin susceptibility are determined by different diagrams, but particularly because the NSLR rate is a local response defined by an integral over all wavelengths, while the spin susceptibility is a global response obtained from the limit $q\rightarrow 0$. The relative corrections to the spin susceptibility as a function of the magnetic field are shown in Figs. 5 and 6 (denoted by ''susceptibility'').

A. Results: Magnetic field and temperature dependence

Unlike the NSLR rate, the Pauli spin susceptibility is not very sensitive to either impurity scattering or order-parameter symmetry, as can be seen in Figs. 5 and 6 for the magnetic-field dependence of the susceptibility. Note that the small constant offsets have to be subtracted off and are included with the leading-order terms as discussed in Sec. III A. The temperature dependence of the fluctuation corrections to χ_s for s-wave pairing is shown in Fig. 20 for different magnetic fields.

The shift in the divergence reflects the field dependence of $T_c(b)$. In Fig. 21 we show for comparison the magnetic field dependence of the fluctuation corrections for s-wave and d-wave symmetry. As can be seen in this figure, the fluctuation corrections to χ_s are insensitive to the order-
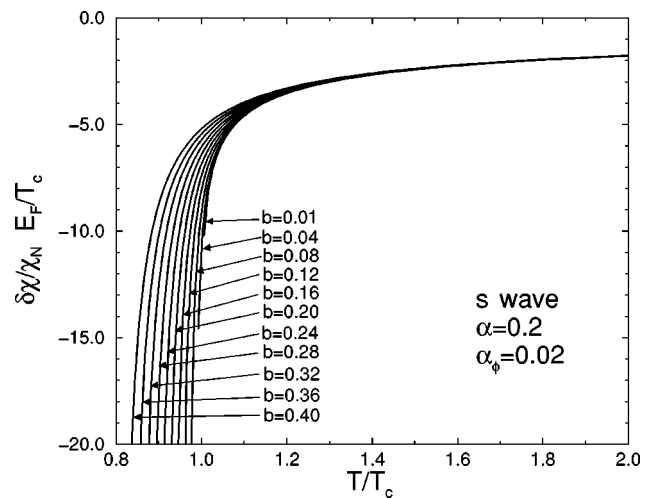

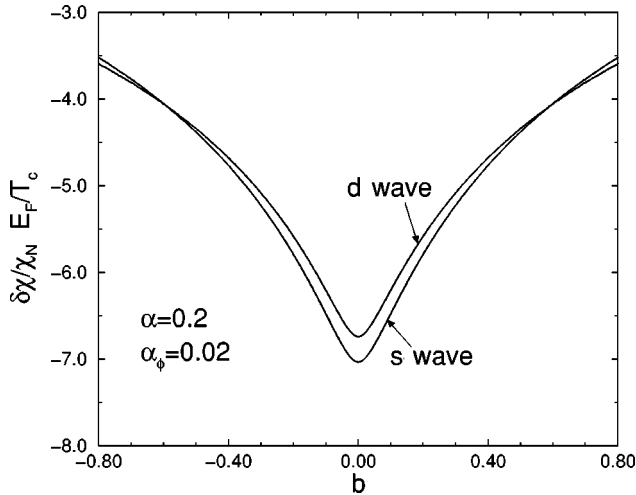FIG. 20. Temperature dependence of fluctuation corrections to Pauli spin susceptibility for different fields.

FIG. 21. Field dependence of fluctuation corrections to Pauli spin susceptibility for $T/T_c = 95\,\text{K}/92.5\,\text{K} \approx 1.03$, and for s- and d-wave pairing.

FIG. 22. Calculations for 2D d-wave pairing fluctuation corrections to the spin susceptibility for $B = 0-14\,\text{T}$ (in steps of 2 T). Shown is the inverse of the derivative $(dK_{spin}/dT)^{-1}$. Circles show measurements of the Knight shift of ^{17}O(2,3) in optimally doped YBCO at 8.4 T.[2] Open circles denote points used for the fit to $K_{spin}(T)$.

parameter symmetry, at least for spin-singlet pairing fluctuations. Thus the mixing of s- and d-wave pairing fluctuations due to orthorhombic anisotropy, which has a profound effect on the fluctuation corrections to the NSLR rate at low field, has almost no effect on the fluctuation corrections to the spin susceptibility.

B. Comparison with experiment

Knight shift measurements in high magnetic fields provide valuable information on the fluctuation contributions to the Pauli spin susceptibility. The effect of static long-wavelength fluctuations on the Pauli susceptibility in zero field have been calculated in three dimensions[30] and two dimensions[7] for $\epsilon = (T - T_c)/T_c \ll 1$. The fluctuation contribution to the spin susceptibility was found to scale as $\delta\chi/\chi_N \sim \ln(\epsilon)$ in 2D, and $\delta\chi/\chi_N \sim \text{const} + \sqrt{\epsilon}$ in 3D. For the 2D case one obtains $(d\delta\chi/dT)^{-1} \sim T - T_c$, and $(d\delta\chi/dT)^{-1} \sim \sqrt{T - T_c}$ for the 3D case. Neither of these limiting cases is consistent with the recent data of Bachman et al.[2] on optimally doped YBCO shown in Fig. 22. These NMR measurements of the Pauli spin susceptibility do not show singular behavior near the transition. This is typical for a fluctuation-dominated crossover transition.[2] For this reason it is preferable to treat the mean-field transition temperature $T_c(H)$ as a fitting parameter. The mean-field transition temperature was determined by analyzing the high-precision measurements of ^{17}O(2,3) Knight shift in optimally doped YBCO at high magnetic fields.[2]

The curvature shown in Fig. 22 is not reproduced by 2D static fluctuations in the low-field limit. Three-dimensional fluctuations to not account for the behavior because they produce curvature in the opposite direction compared to the curves in Fig. 22. We can describe the behavior in Fig. 22 qualitatively and quantitatively by taking into account dynamical fluctuations and orbital quantization. The magnetic field is in a range where neither the low-field approximation nor the lowest-Landau-level approximation is applicable. We perform the sum over the Landau levels and over the dynamical modes numerically. Orbital quantization is the main
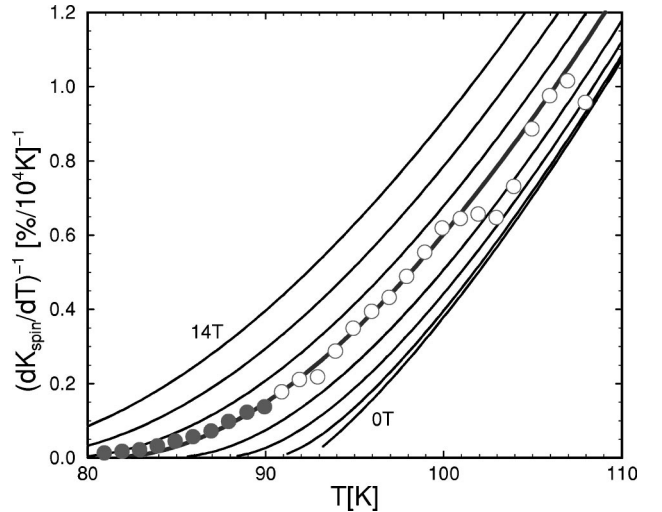
source of the observed curvature at higher fields. Dynamical fluctuations produce curvature also for zero field, where orbital quantization is absent.

A quantitative comparison of our calculations with the experimental data of Bachman et al.[2] is shown in Fig. 22. The fit was performed in the region $T > 90\,\text{K}$ directly on the susceptibility data (open circles). Then the inverse of the derivative of the experimental data and the theoretical curves were calculated; they are extremely sensitive to variations at high temperatures where the Pauli susceptibility deviates very little from a constant. As can be seen in the Fig. 22, the agreement is excellent even up to temperatures of 102 K. The same fit accounts for the data in the nonfitted region (full circles) down to 85 K. The theoretical mean-field temperature was determined to be about 81 K at 8.4 T. As we discussed in Fig. 21, mixing of an s-wave contribution due to orthorhombic anisotropy in YBCO has little influence on the fluctuation corrections to the Pauli spin susceptibility.

V. CONCLUSIONS

We have calculated the pairing fluctuation corrections to the nuclear spin-lattice relaxation rate and to the Pauli spin susceptibility in 2D s-wave and d-wave high-T_c superconductors in strong magnetic fields. Our calculations include dynamical and short-wavelength fluctuations. We account qualitatively and quantitatively for recent experiments performed on optimally doped YBCO solely in terms of d-wave pairing fluctuations, assuming reasonable scattering parameters. We find no necessity to invoke the existence of a spin-density fluctuation pseudogap. We have shown that incorporating orthorhombic anisotropy and the allowed mixing of s-wave and d-wave pairing fluctuation channels leads to a low-field crossover from predominantly s-wave fluctuations to predominantly d-wave fluctuations which provides a natural explanation for the observed evolution from the NQR rate to the low-field (below 2 T) ^{63}Cu NSLR rate on optimally

doped YBCO. We suggest that a change in sign of the fluctuation corrections to the NSLR rate near $T_c(H)$ with increasing field should be observable in the electron doped compounds like $Nd_{2-x}Ce_xCuO_{4-\delta}$, if they have s-wave pairing symmetry. Observation of this effect would be a strong confirmation of s-wave pairing in these compounds.

ACKNOWLEDGMENTS

APPENDIX A: IRREDUCIBLE PAIR SUSCEPTIBILITIES FOR D-WAVE SYMMETRY

In this section we summarize expressions for the ξ-integrated Fermi-surface averages of the product Green's functions at real energies for the case of d-wave pairing in 2D, i.e., $\eta(\psi) = \sqrt{2}\cos 2\psi$. The integrals are related to Eq. (4) by analytic continuation. For d-wave pairing they are

$$A_0(\epsilon,q) = \frac{2\pi N_F}{\sqrt{(v_F q)^2 - (2\tilde{\epsilon})^2}}, \tag{A1}$$

$$A_1(\epsilon,q,\phi) = A_0(\epsilon,q)\frac{-2i\tilde{\epsilon} - \sqrt{(v_F q)^2 - (2\tilde{\epsilon})^2}}{-2i\tilde{\epsilon} + \sqrt{(v_F q)^2 - (2\tilde{\epsilon})^2}}\sqrt{2}\cos 2\phi, \tag{A2}$$

$$A_2(\epsilon,q,\phi) = A_0(\epsilon,q)$$
$$\times\left[1 + \left(\frac{-2i\tilde{\epsilon} - \sqrt{(v_F q)^2 - (2\tilde{\epsilon})^2}}{-2i\tilde{\epsilon} + \sqrt{(v_F q)^2 - (2\tilde{\epsilon})^2}}\right)^2\cos 4\phi\right], \tag{A3}$$

$$[A_1^2 - A_2 A_0](\epsilon,q) = -A_0(\epsilon,q)^2$$
$$\times\left[1 - \left(\frac{-2i\tilde{\epsilon} - \sqrt{(v_F q)^2 - (2\tilde{\epsilon})^2}}{-2i\tilde{\epsilon} + \sqrt{(v_F q)^2 - (2\tilde{\epsilon})^2}}\right)^2\right], \tag{A4}$$

with $\tilde{\epsilon} = \epsilon + i\pi T_c(\alpha + \alpha_\phi)$.

For isotropic s-wave pairing fluctuations we have trivially $A_0(\epsilon,q) = A_1(\epsilon,q) = A_2(\epsilon,q)$ given in Eq. (A1).

APPENDIX B: COHERENCE LENGTHS AND T_c REDUCTION

In the long-wavelength, low-frequency limit the pair fluctuation propagator for s- and d-wave symmetry becomes[10]

$$L_s(q,\omega) = N_F^{-1}\frac{1}{\epsilon_s + \xi_s^2 q^2 - i\omega\tau_s}, \tag{B1}$$

$$L_d(q,\omega) = N_F^{-1}\frac{1}{\epsilon_d + \xi_d^2 q^2 - i\omega\tau_d}. \tag{B2}$$

This result is obtained by expanding Eq. (14) for small q and ω and carrying out the ϵ integral. We define $\alpha_0 = \alpha + \alpha_\phi$, then

$$\frac{\xi_s^2}{\xi_0^2} = \frac{\Psi\left(\frac{1}{2} + \frac{\alpha_\phi T_c}{2T}\right) - \Psi\left(\frac{1}{2} + \frac{\alpha_0 T_c}{2T}\right) + \frac{\alpha T_c}{2T}\Psi'\left(\frac{1}{2} + \frac{\alpha_\phi T_c}{2T}\right)}{2\alpha^2}, \tag{B3}$$

$$\frac{\xi_d^2}{\xi_0^2} = \frac{T_c^2}{T^2}\frac{\left|\Psi''\left(\frac{1}{2} + \frac{\alpha_0 T_c}{2T}\right)\right|}{16}, \tag{B4}$$

$$\tau_s = \frac{\Psi'\left(\frac{1}{2} + \frac{\alpha_\phi T_c}{2T}\right)}{4\pi T}, \tag{B5}$$

$$\tau_d = \frac{\Psi'\left(\frac{1}{2} + \frac{\alpha_0 T_c}{2T}\right)}{4\pi T}, \tag{B6}$$

$$\epsilon_s = \ln\frac{T}{T_c} - \Psi\left(\frac{1}{2} + \frac{\alpha_\phi}{2}\right) + \Psi\left(\frac{1}{2} + \frac{\alpha_\phi T_c}{2T}\right), \tag{B7}$$

$$\epsilon_d = \ln\frac{T}{T_c} - \Psi\left(\frac{1}{2} + \frac{\alpha_0}{2}\right) + \Psi\left(\frac{1}{2} + \frac{\alpha_0 T_c}{2T}\right). \tag{B8}$$

Note that s- and d-wave results differ by more than the replacement of α_ϕ by $\alpha_\phi + \alpha$. The relative influence of α and α_ϕ on the reduction of the coherence length is different for d-wave and s-wave symmetry.

The reduction of T_c by impurity scattering is given by the Abrikosov-Gorkov formulas[15]

$$\ln \frac{T_c}{T_{c0}} - \Psi\left(\frac{1}{2}\right) + \Psi\left(\frac{1}{2} + \frac{\alpha_\phi}{2}\right) = 0 \quad (s \text{ wave}) \quad \text{(B9)}$$

$$\ln \frac{T_c}{T_{c0}} - \Psi\left(\frac{1}{2}\right) + \Psi\left(\frac{1}{2} + \frac{\alpha_0}{2}\right) = 0 \quad (d \text{ wave}). \quad \text{(B10)}$$

APPENDIX C: CLASSIFICATION OF DIAGRAMS

The essential feature for our classification scheme of diagrams is a separation of energy scales. The *low-energy scale* set by the temperature ($k_B T$), the quasiparticle excitation energy (ϵ), the pair excitation energy (ω), the scattering rates ($\hbar/\tau, \hbar/\tau_\phi$), etc., should be well separated from the characteristic *high-energy scales* of the metal, e.g., the Fermi energy (E_F). These energies define a formal expansion parameter given by the ratio of a typical low-energy scale and a typical high-energy scale, for instance, $k_B T_c / E_F$. Alternatively one can write the formal expansion parameter in terms of the ratio of a typical atomic length scale (k_F^{-1}, $\hbar v_F / E_F$, etc.) and a typical long-wavelength scale ($\xi_0 = \hbar v_F / 2\pi k_B T_c$, $l = v_F \tau$, $l_\phi = v_F \tau_\phi$, etc). We perform a systematic expansion in terms of these parameters, and derive all leading fluctuation corrections in the framework of the Green's-functions technique. All diagrams presented here are understood as containing renormalized elements. Thus low-energy fermion Green's functions are *quasiparticle* Green's functions, vertices are renormalized by high-energy quantities. More detailed descriptions of this renormalization procedure are given in Refs. 31–33. We assign for simplicity the order of magnitude *small* to the set of expansion parameters (e.g., *small* $= T_c / E_F$). To estimate the order of magnitude of the diagrams we replace the Green's functions for the quasiparticles by piecewise constant functions, which are equal to $1/small$ if both the momenta are located in a narrow shell of thickness *small* around the Fermi surface and the energies are small, $\epsilon < small$. The corresponding part of phase space is called *low-energy region*. Outside of this phase space area, in the *high-energy region*, we assign to the phase space area a measure of 1, and the high-energy Green's functions are set equal to 1. Analogously, the low-energy range of a pair fluctuation mode consists of small pair excitation energies $\hbar\omega < small$, and small pair momenta $|\mathbf{q}| < small$. Performing the trivial integrations over the steplike Green's functions in the asymptotic limit $small \to 0$ gives the order of the diagram. This is done in the following steps:

(1) Estimate the integrand from the number of quasiparticle lines in the diagram, n_Q, which gives a factor $small^{-(n_Q)}$.
(2) Labeling of the diagram respecting energy and momentum conservation.
(3) Estimate the phase space factors:
    (a) Restricting all energies to their low-energy region

gives a factor $small^{(n_E)}$, where n_E is the number of independent internal energies.

    (b) Restricting the pair momentum to its low-energy region gives a factor $small^D$ for every quasiparticle pair in the fluctuation channel, which is not otherwise restricted to the low-energy region. The physical dimension D enters explicitly.

    (c) Restricting all remaining fermion momenta to their low-energy region is the only nontrivial part of the estimate. The number of restrictions n_K gives a factor $small^{(n_K)}$. Note that the sum of two low-energy momenta is not necessarily in the low-energy region again. One needs additional geometrical restrictions to the angles between the momenta.

The leading-order corrections in 2D to the NSRL rate are determined by the diagrams in Fig. 2 for short-wavelength external perturbations $\hbar q_e \sim p_F$, while the leading-order corrections in 2D to the spin susceptibility are determined by the diagrams in Fig. 19 for long-wavelength external perturbations $\hbar q_e \ll p_F$.

In three dimensions these corrections are another order higher in *small*, showing the insignificance of fluctuations in conventional 3D superconductors. In one dimension they are of leading order, signaling the breakdown of the quasiparticle picture.

APPENDIX D: CORRECTIONS TO THE PARTICLE-HOLE SUSCEPTIBILITY

We use a shorthand notation, for the combined (bosonic) Matsubara energy and momentum of the the pairing fluctuation mode: $Q \equiv (\omega_l, \mathbf{q})$. Similarly, $P \equiv (\epsilon_n, \mathbf{p})$, $P' \equiv (\epsilon_{n'}, \mathbf{p'})$, $Q - P \equiv (\omega_l - \epsilon_n, \mathbf{q} - \mathbf{p})$, $\Sigma_P \equiv T\Sigma_n \Sigma_\mathbf{p}$, etc. We use the usual Feynman rules for evaluating diagrams.[15] Although we consider spin-singlet, s- or d-wave pairing, both spin-singlet and spin-triplet fluctuation channels contribute because of triplet impurity Cooperons. We neglect the Zeeman coupling of the quasiparticle propagators to the magnetic field. This allows us to decompose the vertices and fluctuation propagator in the particle-particle channel into spin-singlet and spin-triplet components:

$$\Gamma_{\alpha\beta\gamma\delta}(P, P', Q) = \Gamma^s(P, P', Q)\sigma^y_{\alpha\beta}\sigma^y_{\gamma\delta} + \Gamma^t(P, P', Q)$$
$$\times (\sigma^y \boldsymbol{\sigma})_{\alpha\beta}(\boldsymbol{\sigma}\sigma^y)_{\gamma\delta}, \quad \text{(D1)}$$

$$K_{\alpha\beta\gamma\delta}(P, P', Q) = K^s(P, P', Q)\sigma^y_{\alpha\beta}\sigma^y_{\gamma\delta} + K^t(P, P', Q)$$
$$\times (\sigma^y \boldsymbol{\sigma})_{\alpha\beta}(\boldsymbol{\sigma}\sigma^y)_{\gamma\delta}. \quad \text{(D2)}$$

The Bethe-Salpeter equation for the fluctuation propagator,

$$K_{\alpha\beta\gamma\delta}(P, P', Q) = \Gamma_{\alpha\beta\gamma\delta}(P, P', Q)$$
$$+ \frac{T}{2}\sum_{\epsilon,\eta}\sum_{P''}\Gamma_{\alpha\beta\eta\epsilon}(P, P'', Q) \cdot G(P'')$$
$$\times G(Q - P'') \cdot K_{\epsilon\eta\gamma\delta}(P'', P', Q), \quad \text{(D3)}$$

separates into singlet and triplet channels:

$$K^{s,t}(P,P',Q) = \Gamma^{s,t}(P,P',Q) + T \cdot \sum_{P''} \Gamma^{s,t}(P,P'',Q) G(P'')$$

$$\times G(Q-P'') \cdot K^{s,t}(P'',P',Q). \tag{D4}$$

Corrections to the NSLR rate are described by the diagrams in Fig. 2. The first diagram was investigated by Maki and Thompson,[9] and the last two diagrams represent contributions to the NSLR rate from fluctuation contributions to the quasiparticle density of states. Particle-hole vertex corrections, labeled ''V'' in Fig. 2, can be neglected to leading order in T_c/E_F above T_c because they are all proportional to $\int d\xi_{\mathbf{k}} G(\epsilon_n,\xi_{\mathbf{k}})^2 \approx 0$. The expressions corresponding to the diagrams in Fig. 2, with external Matsubara energy ω_m, are then [we use $W \equiv (\omega_m, \mathbf{q}')$]

$$\chi_{MT}(\omega_m) = \sum_{\alpha\beta\gamma\delta} \sum_{PQ\mathbf{q}'} (\boldsymbol{\sigma}_{\delta\alpha}\mathbf{A}_{-P,W-P})(\boldsymbol{\sigma}_{\gamma\beta}\mathbf{A}_{P,P-W})$$

$$\times G(P-W)G(P)G(Q-P)$$

$$\times G(Q-P+W)K_{\alpha\beta\gamma\delta}(P,P-W,Q)$$

$$= -2\sum_{PQ\mathbf{q}'} |\mathbf{A}_{P,P-W}|^2 G(P-W)G(P)$$

$$\times G(Q-P)G(Q-P+W)[K^s(P,P-W,Q)$$

$$- K^t(P,P-W,Q)], \tag{D5}$$

$$\chi_{DOS}(\omega_m) = \sum_{\alpha\beta\gamma} \sum_{PQ\mathbf{q}'} (\boldsymbol{\sigma}_{\alpha\gamma}\mathbf{A}_{P-W,P})(\boldsymbol{\sigma}_{\gamma\alpha}\mathbf{A}_{P,P-W})$$

$$\times [G(P-W)+G(P+W)]G(P)^2$$

$$\times G(Q-P)K_{\alpha\beta\beta\alpha}(P,P,Q)$$

$$= 4\sum_{PQ\mathbf{q}'} |\mathbf{A}_{P-W,P}|^2 [G(P-W)$$

$$+ G(P+W)]G(P)^2 G(Q-P)[K^s(P,P-W,Q)$$

$$+ 3K^t(P,P-W,Q)]. \tag{D6}$$

The term χ_{MT} corresponds to the Maki-Thompson diagram, (a) in Fig. 2, and the second term, χ_{DOS}, to the two DOS diagrams, (b) and (c) in Fig. 2. We use the relations $\mathbf{A}_{-P,-P'} = (\mathbf{A}_{P,P'})^*$ and $\mathbf{A}_{P',P} = (\mathbf{A}_{P,P'})^*$ to simplify the results.

The fluctuation corrections to the Pauli spin susceptibility are obtained from the diagrams in Fig. 19:

$$\chi_{MT}(0) = \sum_{\alpha\beta\gamma\delta} \sum_{PQ} (\mathbf{h}\cdot\boldsymbol{\sigma}_{\delta\alpha})(\mathbf{h}\cdot\boldsymbol{\sigma}_{\gamma\beta})G(P)^2$$

$$\times G(Q-P)^2 K_{\alpha\beta\gamma\delta}(P,P,Q)$$

$$= -2\sum_{PQ} G(P)^2 G(Q-P)^2$$

$$\times [K^s(P,P,Q) - K^t(P,P,Q)], \tag{D7}$$

$$\chi_{DOS}(0) = 2\sum_{\alpha\beta\gamma} \sum_{PQ} (\mathbf{h}\cdot\boldsymbol{\sigma}_{\alpha\gamma})(\mathbf{h}\cdot\boldsymbol{\sigma}_{\gamma\alpha})G(P)^3$$

$$\times G(Q-P)K_{\alpha\beta\beta\alpha}(P,P,Q)$$

$$= 4\sum_{PQ} G(P)^3 G(Q-P)$$

$$\times [K^s(P,P,Q) + 3K^t(P,P,Q)], \tag{D8}$$

$$\chi_{AL}(0) = \sum_{\alpha\beta\gamma\delta\eta\zeta} \sum_{PP'Q} (\mathbf{h}\cdot\boldsymbol{\sigma}_{\zeta\alpha})(\mathbf{h}\cdot\boldsymbol{\sigma}_{\eta\beta})G(P)^2 G(P')^2$$

$$\times G(Q-P)G(Q-P')K_{\alpha\beta\gamma\delta}(P,P',Q)$$

$$\times K_{\delta\gamma\eta\zeta}(P',P,Q)$$

$$= 4\sum_{PP'Q} G(P)^2 G(P')^2$$

$$\times G(Q-P)G(Q-P')[K^s(P,P',Q)K^t(P',P,Q)$$

$$+ K^t(P,P',Q)K^s(P',P,Q)]. \tag{D9}$$

The first term, $\chi_{MT}(0)$, corresponds to diagram (a) in Fig. 19 (Maki-Thompson), the second term, $\chi_{DOS}(0)$, to diagrams (b) and (c) (DOS) and the last term, $\chi_{AL}(0)$, to the Aslamazov-Larkin diagram, (d) in Fig. 19. Particle-hole vertex corrections, labeled ''V'' in Fig. 19, can be neglected for similar reasons as in the case of the NSLR rate.

To evaluate momentum integrals we split the $\mathbf{p}$ sum into a $\xi_{\mathbf{p}}$ integral and a Fermi-surface average (we use the notation $\langle\cdots\rangle_{\mathbf{p}} := \int dp_F n(p_F)\cdots$ where $n(p_F)$ is the angle-resolved (normalized) density of states at the Fermi surface). Thus

$$\sum_{\mathbf{p}} \approx N_F \cdot \int_{-\infty}^{\infty} d\xi_{\mathbf{p}} \cdot \langle\cdots\rangle_{\mathbf{p}}. \tag{D10}$$

The lower limit of the integrals is extended from $-\mu$ to $-\infty$. This approximation induces corrections of order T_c/E_F which vary on a temperature (and field) scale large compared to T_c and can be incorporated in the asymptotic normal state behavior as discussed in Sec. III A. We use the abbreviations

$$\underline{G}_1(P) = N_F \int d\xi_{\mathbf{p}} G(P), \tag{D11}$$

$$\underline{G}_2(P,Q) = N_F \int d\xi_{\mathbf{p}} G(P)G(Q-P), \tag{D12}$$

$$\underline{G}_3(P,Q) = N_F \int d\xi_{\mathbf{p}} G(P)^2 G(Q-P), \tag{D13}$$

$$\underline{G}_{3'}(P,Q) = N_F \int d\xi_{\mathbf{p}} G(P)G(Q-P)^2, \tag{D14}$$

$$\underline{G}_4(P,Q) = N_F \int d\xi_{\mathbf{p}} G(P)^3 G(Q-P), \tag{D15}$$

$$\underline{G}_{4'}(P,Q) = N_F \int d\xi_{\mathbf{p}} G(P)^2 G(Q-P)^2. \tag{D16}$$

These expressions can be evaluated by complex integration. After ξ integration (as on the left-hand sides of the above equations) the momenta are confined to the Fermi surface. The formal identity

$$(G[\Sigma(\epsilon_n)](P))^{m+1} = \frac{1}{m!}\left(\frac{\delta}{\delta\Sigma(\epsilon_n)}\right)^m G[\Sigma(\epsilon_n)](P),$$

(D17)

where $\Sigma(\epsilon_n)$ is the self-energy for the Green's function, implies

$$\underline{G}_{2+m}[\Sigma(\epsilon_n),\Sigma(\omega_l-\epsilon_n)](P,Q)$$
$$= \frac{1}{m!}\left(\frac{\delta}{\delta\Sigma(\epsilon_n)}\right)^m \underline{G}_2[\Sigma(\epsilon_n),\Sigma(\omega_l-\epsilon_n)](P,Q).$$

(D18)

Because the functional dependence of $\underline{G}_2$ on the self-energies contains only the combination $\Sigma(\epsilon_n)-\Sigma(\omega_l-\epsilon_n)$, we obtain the relations $\underline{G}_{4'}=-2\underline{G}_4$ and $\underline{G}_{3'}=-\underline{G}_3$.

In the weak-coupling theory for pair fluctuations we have $K^s(P,P',Q)\equiv K(P,P',Q)=\tilde{\eta}(P,Q)L(Q)\tilde{\eta}(P',Q)$, and we can replace $K^t(P,P',Q)$ and $K^t(P',P,Q)$ in the Aslamazov-Larkin diagram by $C(\epsilon_n,Q)[\delta(\epsilon_{n'}-\epsilon_n)-\delta(\omega_l-\epsilon_{n'}-\epsilon_n)]/2$. The quantities $\tilde{\eta}$, L and C are defined in Sec. II. We neglect diagrams containing only impurity interactions (and no pairing interaction), which describe pure weak-localization effects. Furthermore, we assume that the hyperfine matrix elements are isotropic on the Fermi surface. Thus we obtain for the NSLR rate

$$\chi_{MT}(\omega_m) = -2\cdot|\mathbf{A}|^2\cdot\sum_{\epsilon_n,Q}\langle\tilde{\eta}(P,Q)\underline{G}_2(P,Q)\rangle_\mathbf{p}$$
$$\times\langle\tilde{\eta}(P-W,Q)\underline{G}_2(P-W,Q)\rangle_{\mathbf{p}-\mathbf{q'}}\cdot L(Q),$$

(D19)

$$\chi_{DOS}(\omega_m) = 4\cdot|\mathbf{A}|^2\cdot\sum_{\epsilon_n,Q}\langle\tilde{\eta}(P,Q)^2\underline{G}_3(P,Q)\rangle_\mathbf{p}$$
$$\times\langle\underline{G}_1(P-W)\rangle_{\mathbf{p}-\mathbf{q'}}\cdot L(Q),$$

(D20)

and for the Pauli susceptibility

$$\chi_{MT+DOS}(0) = 8\cdot\sum_{\epsilon_n,Q}\langle\tilde{\eta}(P,Q)^2\underline{G}_4(P,Q)\rangle_\mathbf{p}\cdot L(Q),$$

(D21)

$$\chi_{AL}(0) = 8\cdot\sum_{\epsilon_n,Q}(\langle\tilde{\eta}(P,Q)\underline{G}_3(P,Q)\rangle_\mathbf{p})^2\cdot C(\epsilon_n,Q)\cdot L(Q).$$

(D22)

These results can be written more compactly using the identities

$$\left\langle\tilde{\eta}(P,Q)^2\frac{\delta}{\delta\Sigma(\epsilon_n)}\underline{G}_2(P,Q)\right\rangle_\mathbf{p}$$
$$= \frac{\delta}{\delta\Sigma(\epsilon_n)}\langle\eta(\mathbf{p})\tilde{\eta}(P,Q)\underline{G}_2(P,Q)\rangle_\mathbf{p},$$

(D23)

$$\left\langle\tilde{\eta}(P,Q)^2\frac{\delta^2}{\delta\Sigma(\epsilon_n)^2}\underline{G}_2(P,Q)\right\rangle_\mathbf{p}$$
$$+ 2\left\langle\tilde{\eta}(P,Q)\frac{\delta}{\delta\Sigma(\epsilon_n)}\underline{G}_2(P,Q)\right\rangle_\mathbf{p}^2 C(\epsilon_n,Q)$$
$$= \frac{\delta^2}{\delta\Sigma(\epsilon_n)^2}\langle\eta(\mathbf{p})\tilde{\eta}(P,Q)\underline{G}_2(P,Q)\rangle_\mathbf{p}.$$

(D24)

(D25)

Defining $G_1(\epsilon_n)=\langle\underline{G}_1(P)\rangle_\mathbf{p}$, $B_1(\epsilon_n,Q)=\langle\tilde{\eta}(P,Q)\underline{G}_2(P,Q)\rangle_\mathbf{p}$, and $B_2(\epsilon_n,Q)=\langle\eta(\mathbf{p})\tilde{\eta}(P,Q)\underline{G}_2(P,Q)\rangle_\mathbf{p}$ we obtain for the NSLR rate

$$\chi_{MT}(\omega_m) = -2\cdot|\mathbf{A}|^2\cdot\sum_{\epsilon_n,Q}B_1(\epsilon_n,Q)B_1(\epsilon_n-\omega_m,Q)\cdot L(Q),$$

(D26)

$$\chi_{DOS}(\omega_m) = 4\cdot|\mathbf{A}|^2\cdot\sum_{\epsilon_n,Q}G_1(\epsilon_n-\omega_m)\frac{\delta}{\delta\Sigma(\epsilon_n)}$$
$$\times B_2(\epsilon_n,Q)\cdot L(Q),$$

(D27)

and for the Pauli susceptibility

$$\chi_{MT+DOS+AL}(0) = 4\cdot\sum_{\epsilon_n,Q}\frac{\delta^2}{\delta\Sigma(\epsilon_n)^2}B_2(\epsilon_n,Q)\cdot L(Q).$$

(D28)

[1] V. F. Mitrović, H. N. Bachman, W. P. Halperin, M. Eschrig, J. A. Sauls, A. P. Reyes, P. Kuhns, and W. G. Moulton, Phys. Rev. Lett. **82**, 2784 (1999).

[2] H. N. Bachman, V. F. Mitrović, A. P. Reyes, W. P. Halperin, M. Eschrig, J. A. Sauls, A. Kleinhammes, P. Kuhns, and W. G. Moulton (unpublished).

[3] D. S. Fisher, M. P. A. Fisher, and D. A. Huse, Phys. Rev. B **43**, 130 (1991); G. Blatter, M. V. Feigel'man, V. B. Geshkenbein, A. I. Larkin, and V. M. Vinokur, Rev. Mod. Phys. **66**, 1125 (1994).

[4] A. Rigamonti, F. Borsa, and P. Carretta, Rep. Prog. Phys. **61**, 1367 (1998).

[5] K. Kuboki and H. Fukuyama, J. Phys. Soc. Jpn. **58**, 376 (1989).

[6] J. Heym, J. Low Temp. Phys. **89**, 869 (1992).

[7] M. Randeria and A. A. Varlamov, Phys. Rev. B **50**, 10 401 (1994).

[8] P. Carretta, D. V. Livanov, A. Rigamonti, and A. A. Varlamov, Phys. Rev. B **54**, R9682 (1996).

[9] K. Maki, Prog. Theor. Phys. **40**, 193 (1968); R. S. Thompson, Phys. Rev. B **1**, 327 (1970); Physica (Amsterdam) **55**, 296 (1971).

[10] A. A. Varlamov, G. Balestrino, E. Milani, D. V. Livanov, cond-mat/9710175v2, Adv. Phys. (to be published).

[11] M. Randeria, in *Precursor Pairing Correlations and Pseudogaps*, Proceedings of the International School of Physics "Enrico Fermi," Course CXXXVI, Varenna, 1997, edited by G. Iadorisi and J. R. Schrieffer, cond-mat/9710223 (IOS Press, Amsterdam, in press).

[12] A. V. Chubukov, D. Pines, and B. Stojkovic, J. Phys.: Condens. Matter **8**, 1 (1996).

[13] T. Auler, M. Horvatić, J. A. Gillet, C. Berthier, Y. Berthier, P. Ségransan, and J. Y. Henry, Phys. Rev. B **56**, 11 294 (1997).

[14] K. Aoi, R. Meservey, and P. M. Tedrow, Phys. Rev. B **9**, 875 (1974).

[15] A. A. Abrikosov, L. P. Gorkov, and I. E. Dzyaloshinski, *Methods of Quantum Field Theory in Statistical Physics* (Prentice-Hall, Englewood Cliffs, NJ, 1963).

[16] A. A. Abrikosov and L. P. Gorkov, Zh. Éksp. Teor. Fiz. **39**, 1781 (1960) [Sov. Phys. JETP **12**, 1243 (1961)].

[17] D. B. Tanner and T. Timusk, in *Physical Properties of High Temperature Superconductors*, edited by D. M. Ginsberg (World Scientific, Singapore, 1992), Vol. III.

[18] V. V. Dorin, R. A. Klemm, A. A. Varlamov, A. I. Buzdin, and D. V. Livanov, Phys. Rev. B **48**, 12 951 (1993).

[19] M. Eschrig, J. Heym, and D. Rainer, J. Low Temp. Phys. **95**, 323 (1994).

[20] The critical value for α_ϕ in the dirty limit for isotropic s-wave pairing symmetry, corresponding to a change in the sign for the divergence of the corrections to NSLR rate for $T \to T_c$, is given by the solution of the equation (Ψ denotes the digamma function)

$$\Psi'\left(\frac{1}{2}+\frac{\alpha_\phi}{2}\right)=-\frac{3}{2}\alpha_\phi\Psi''\left(\frac{1}{2}+\frac{\alpha_\phi}{2}\right),$$

which gives $\alpha_{\phi,crit}\approx 0.258$ (M. Eschrig, Diploma thesis, Universität Bayreuth, 1994).

[21] C. P. Slichter, *Priciples of Magnetic Resonance*, 3rd ed. (Springer, New York, 1990).

[22] G. M. Eliashberg, Zh. Éksp. Teor. Fiz. **61**, 1254 (1971) [Sov. Phys. JETP **34**, 668 (1972)].

[23] J. Kurkijärvi, V. Ambegaokar, and G. Eilenberger, Phys. Rev. B **5**, 868 (1972); P. A. Lee and M. G. Payne, *ibid.* **5**, 923 (1972).

[24] The anomalous MT term [see Eq. (30), last line], is determined by $|B_1|^2$, which is equal to $|A_1|^2$ for d-wave pairing and $|A_0|^2$ for s-wave pairing in the clean limit. Because $|A_0|^2 \sim |(v_F q)^2 - (2\tilde\epsilon)^2|^{-1}$ the dominant contribution comes from the region $2\tilde\epsilon \approx v_F q$ in the clean limit for s-wave pairing. For this region from Eq. (A2) in Appendix A follows $|A_1(\epsilon,q,\phi)|^2 \approx 2(\cos 2\phi)^2|A_0(\epsilon,q,\phi)|^2$, so that in the clean limit the anomalous MT term for d-wave pairing gives results similar to the s-wave case, i.e., a large positive contribution. The regular MT term, on the other hand, contains the quantity $(A_1)^2$. A principal-value integral leads to a result which is proportional to $(v_F q)^4$ for d-wave pairing and is negligible as can be seen in Fig. 6. With

impurity scattering, the imaginary part of $\tilde\epsilon$ leads to suppression of the anomalous MT term.

[25] In d-wave symmetry different Landau levels are coupled through higher-order terms in the pair momentum operator **q**. This effect is unimportant except possibly in very high fields near $H_{c2}(0)$. In typical high-field experiments $H \lesssim 30$ T is still much lower than $H_{c2}(0)$. To determine the mean-field transition temperature in a finite magnetic field we averaged B_2 over ϕ for d-wave pairing to eliminate the ϕ dependence in the fourth- and higher-order terms in the momentum.

[26] A. J. Millis, H. Monien, and D. Pines, Phys. Rev. B **42**, 167 (1990); N. Bulut, D. W. Hone, D. J. Scalapino, and N. E. Bickers, *ibid.* **41**, 1797 (1990), T. Moriya, Y. Takahashi, and K. Ueda, J. Phys. Soc. Jpn. **52**, 2905 (1990).

[27] P. Bourges, H. Casalta, L. P. Regnault, J. Bossy, P. Burlet, C. Vettier, E. Beaugnon, P. Gautier-Picard, and R. Tournier, Physica C **234-236**, 830 (1997).

[28] Y.-Q. Song, Ph.D. thesis, Northwestern University, 1991.

[29] We use compact diagrams for our diagrammatic representation. The standard way of drawing diagrams is obtained by resolving the internal structure of the K-vertices and assigning explicit spin labels. The set of four diagrams shown in Fig. 19 is equivalent to the set of ten diagrams given, e.g., in Ref. 10. We demonstrate this connection for the compact form of the Aslamazov-Larkin diagram. It contains for singlet pairing only one pair propagator. The other collective mode is a Cooperon-type impurity ladder in the particle-particle channel. One obtains four different diagrams of this type. In Ref. 10 they are referred to also as special types of Maki-Thompson and DOS diagrams (counting only pairing fluctuation modes for diagram naming schemes). The Aslamazov-Larkin diagram in the noncompact form is exactly zero for spin singlet pairing. The same is true for the corresponding contribution to the NSLR rate, but in this case it is additionally one order smaller in the parameter T_c/E_F.

[30] P. Fulde and S. Strässler, Phys. Rev. B **1**, 3017 (1970).

[31] J. Serene and D. Rainer, Phys. Rep. **101**, 221 (1983).

[32] D. Rainer, in *Progress in Low Temperature Physics X*, edited by D. F. Brewer (Elsevier Science, Amsterdam, 1986).

[33] D. Rainer and J. A. Sauls, in *Superconductivity: From Basic Physics to the Latest Developments*, edited by P. N. Butcher and Yu Lu (World Scientific Publishing, Singapore, 1995).